

1 **A simple object-oriented and open source model for scientific and policy analyses of**  
2 **the global climate system–Hector v1.0**

3 C.A. Hartin\*, P. Patel, A. Schwarber, R.P. Link, and B.P. Bond-Lamberty

4

5 Pacific Northwest National Laboratory, Joint Global Change Research Institute at the  
6 University of Maryland–College Park, 5825 University Research Court, College Park, MD  
7 20740, USA

8

9 \*Corresponding author: [corinne.hartin@pnl.gov](mailto:corinne.hartin@pnl.gov)

10

11

12 **Abstract**

13 Simple climate models play an integral role in the policy and scientific communities.  
14 They are used for climate mitigation scenarios within integrated assessment models,  
15 complex climate model emulation, and uncertainty analyses. Here we describe Hector  
16 v1.0, an open source, object-oriented, simple global climate carbon-cycle model. This  
17 model runs essentially instantaneously while still representing the most critical global  
18 scale earth system processes. Hector has a three-part main carbon cycle: a one-pool  
19 atmosphere, land, and ocean. The model's terrestrial carbon cycle includes primary  
20 production and respiration fluxes, accommodating arbitrary geographic divisions into,  
21 e.g., ecological biomes or political units. Hector actively solves the inorganic carbon  
22 system in the surface ocean, directly calculating air-sea fluxes of carbon and ocean pH.  
23 Hector reproduces the global historical trends of atmospheric [CO<sub>2</sub>], radiative forcing,  
24 and surface temperatures. The model simulates all four Representative Concentration  
25 Pathways with equivalent changes of key variables over time compared to current  
26 observations, MAGICC (a well-known simple climate model), and models from the 5<sup>th</sup>  
27 Coupled Model Intercomparison Project. Hector's flexibility, open source nature, and  
28 modular design will facilitate a broad range of research in various areas.

29

30

31 **1.0 Introduction**

32 Projecting future impacts of anthropogenic perturbations on the climate system  
33 relies on understanding the interactions of key earth system processes. To accomplish  
34 this, a hierarchy of climate models with differing levels of complexity and resolution are  
35 used, ranging from purely statistical or empirical models, to simple energy balance  
36 models, to fully-coupled Earth System Models (ESMs) (Stocker, 2011).

37 Reduced-complexity or simple climate models (SCMs) lie in the middle of this  
38 spectrum, representing only the most critical global scale earth system processes with  
39 low spatial and temporal resolution, e.g., carbon fluxes between the ocean and  
40 atmosphere, primary production and respiration fluxes on land. These models are  
41 relatively easy to use and understand, and are computationally inexpensive. Most SCMs  
42 have a few key features: 1) calculating future concentrations of greenhouse gases  
43 (GHGs) from given emissions while modeling the global carbon cycle; 2) calculating  
44 global mean radiative forcing from greenhouse gas concentrations; and 3) converting  
45 the radiative forcing to global mean temperature (e.g., Wigley, 1991; Meinshausen et al.,  
46 2011a; Tanaka et al., 2007b; Lenton, 2000).

47 With these capabilities, SCMs play an integral role in decision making and scientific  
48 research. For example, energy-economic-climate models or Integrated Assessment  
49 Models (IAMs) are used to address issues on energy system planning, climate mitigation,  
50 stabilization pathways, and land-use changes (Wigley et al., 1996; Edmonds and Smith,  
51 2006; van Vuuren et al., 2011). ESMs are too computationally expensive to use in these

52 analyses. Therefore, all IAMs rely on a simple representation of the global climate  
53 system.

54 Depending on the purpose of the IAMs (economics, cost-benefit analysis, or more  
55 physical based processes), the corresponding climate and carbon component varies in  
56 complexity and resolution. For example, models like DICE, FUND, and MERGE have a  
57 highly simplified carbon/climate system (Nordhaus, 2008; Anthoff and Tol, 2014; Manne  
58 and Richels, 2005). IAMs focusing more on the physical processes of the natural system  
59 and the economy employ more complex representations of the climate/carbon system.  
60 Models like GCAM (Global Change Assessment Model) and MESSAGE use MAGICC as  
61 their SCM (Meinshausen et al., 2011a; Riahi et al., 2007; Calvin et al., 2011). Increasing  
62 in complexity, some IAMs include the climate/carbon system at gridded scales (e.g.,  
63 IMAGE), and can be coupled to earth system models of intermediate complexity (e.g.,  
64 MIT IGSM), or more recently coupled to a full earth system model (the iESM project)  
65 (Bouwman et al., 2006; Sokolov et al., 2005; Bond-Lamberty et al., 2014; Di Vittorio et  
66 al., 2014; Collins et al., 2015).

67 SCMs such as MAGICC, GENIE, and the climate emulation tool at RDCEP are also  
68 used as emulators of more complex ESMs (Meinshausen et al., 2011c; Schlesinger and  
69 Jiang, 1990; Challenor, 2012; Ratto et al., 2012; Lenton et al., 2009; Castruccio et al.,  
70 2014). The behavior of SCMs can be constrained to replicate the overall behavior of the  
71 more complex ESM. For instance, the climate sensitivity of a SCM can be made equal to  
72 that of an ESM by altering a single model parameter. In particular, the MAGICC model  
73 has been central to the analyses presented in the Intergovernmental Panel on Climate

74 Change (IPCC) reports, and can be parameterized to emulate a large suite of ESMs  
75 (Meinshausen et al., 2011a).

76 Lastly, SCMs are computationally efficient and inexpensive to run. Therefore, they  
77 are used to run multiple simulations of future climate change emissions scenarios,  
78 parameter sensitivity experiments, perturbed physics experiments, large ensemble runs,  
79 and uncertainty analyses (Senior and Mitchell, 2000; Hoffert et al., 1980; Harvey and  
80 Schneider, 1985; Ricciuto et al., 2008; Sriver et al., 2012; Irvine et al., 2012). MAGICC,  
81 the Bern CC model, and SNEASY are examples of a few models used for uncertainty  
82 analysis (Meinshausen et al., 2011c; Urban and Keller, 2010; Joos et al., 2001b). SCMs  
83 have been useful in reducing uncertainties in future CO<sub>2</sub> sinks, quantifying parametric  
84 uncertainties in sea-level rise, ice-sheet modeling, ocean-heat uptake, and aerosol  
85 forcing (Ricciuto et al., 2008; Sriver et al., 2012; Applegate et al., 2012; Urban and Keller,  
86 2009).

87 This study introduces Hector v1.0, an open source, object-oriented, simple climate  
88 carbon-cycle model. Hector was developed with three main goals in mind. First, Hector  
89 is an open source model, an important quality given that the scientific community,  
90 funding agencies, and journals are increasingly emphasizing transparency and open  
91 source (E.P. White, 2013; Heron et al., 2013), particularly in climate change sciences  
92 (Wolkovich et al., 2012). A large community of scientists can access, use, and enhance  
93 open source models, with the potential for long-term utilization, improvement, and  
94 reproducibility (Ince et al., 2012). Second, a clean design using an object-oriented  
95 framework is critical for Hector development and future use. This allows for new

96 components to easily be added to Hector, i.e. the model's functionality to be easily  
97 extended in the future. In addition, this framework allows for easy coupling into IAMs,  
98 in particular GCAM. Lastly, Hector is a stand-alone simple climate model used to answer  
99 fundamental scientific research questions, uncertainty analysis, parameter sensitivities,  
100 etc.

101       One of the fundamental questions faced in developing a SCM is how much detail  
102 should be represented in the climate system. Our goal is to introduce complexity only  
103 where warranted, keeping the representations of the climate system as simple as  
104 possible. This results in fewer calculations, faster execution times, and easier analysis  
105 and interpretation of results. Sections 2, 3, and 4 describe the structure and  
106 components of Hector. Sections 5 and 6 describe the experiments, results and  
107 comparison of Hector against observational data and other models (MAGICC and  
108 CMIP5).

109

## 110 **2.0 Model architecture**

### 111 **2.1 Overall structure and design**

112       Hector is written in C++ and uses an object-oriented design that enforces clean  
113 separation between its different parts, which interact via strictly defined interfaces. The  
114 separation keeps each software module self-contained, which makes the code easy for  
115 users to understand, maintain, and enhance. Entities in the model include a command-  
116 line *wrapper*, the model *coupler*, various *components* organized around scientific areas

117 (carbon cycling, radiative forcing, etc.) and *visitors* responsible for model output. Each of  
118 these is discussed below.

## 119 **2.2 Model Coupler**

120 Hector's control flow starts with the coupler, which is responsible for: 1) parsing  
121 and routing input data to the model components; 2) tracking how the components  
122 depend on each other; 3) passing messages and data between components; 4) providing  
123 facilities for logging, time series interpolation, etc.; and 5) controlling the main model  
124 loop as it progresses through time. Any errors thrown by the model are caught by the  
125 wrapper, which prints a detailed summary of the error.

126 Input data are specified in flat text files, and during startup are routed to the  
127 correct model component for its initialization. Some of the key initial model conditions  
128 are summarized in **Table 1 and Table 2**. For more details of initial model conditions we  
129 urge the reader to download Hector v1.0 (<https://github.com/JGCRI/hector>).

130 Components can send messages to each other during the model run, most often  
131 requesting data. The messaging interface is also available to external subroutines, such  
132 as components of IAMs or other linked models. The coupler handles message routing  
133 (via the *capability* mechanism, below) and enforces mandatory type checking: e.g., if a  
134 component requests mean global temperature in °C but the data are provided in K, an  
135 error will be thrown (i.e., execution halts) unless the receiving component can handle  
136 this situation.

137 Visitor patterns are units of code that traverse all model components and handle  
138 model output (Martin et al., 1997). Two visitors currently exist: one saves an easily-

139 readable summary table to an output file, while the other writes a stream of model data  
140 (both standard outputs and internal diagnostics). After the model finishes, this ‘stream’  
141 file can be parsed and summarized by R scripts (R Development Core Team, 2014)  
142 included with Hector. Log files may also be written by any model entity, using facilities  
143 provided by the coupler. The full sequence of events during a model run is summarized  
144 in **Figure 1**.

### 145 **2.3 Components**

146 Model components are submodels that communicate with the coupler. From  
147 the coupler’s point of view, components are fully defined by their *capabilities* and  
148 *dependencies*. At model startup, before the run begins, components inform the coupler  
149 of their capabilities, i.e., what data they can provide to or accept from the larger model  
150 system. The coupler uses this information to route messages, such as requests for data,  
151 between components. Components also register their dependencies, i.e., what results  
152 they require from other components in order to complete their computations. After  
153 initialization, but before the model begins to run, the coupler uses this dependency  
154 information to determine the order in which components will be called in the main  
155 control loop.

156 The model’s modular architecture, and the *capability/dependency* systems  
157 described above, allows swapping, enabling and disabling of model components directly  
158 via the input without recompiling. For example, this means that a user can test two  
159 different ocean submodels and easily compare results without having to rebuild the  
160 model.



161 **2.4 Time step, spinup, and constraints**

162 The model's fundamental time step is 1 year, although the carbon cycle can  
163 operate on a finer resolution when necessary (Section 3.1). When the model is on an  
164 integer date (e.g. 1997.0) it is considered to be the midpoint of that particular calendar  
165 year, in accordance with Representative Concentration Pathway (RCP) data  
166 (Meinshausen et al., 2011b).

167 Like many models, Hector has an optional 'spinup' step, in which the model runs  
168 to equilibrium in an a historical, perturbation-free mode (Pietsch and Hasenauer, 2006).  
169 This occurs after model initialization, but before the historical run begins, and ensures  
170 that the model is in steady state when it enters the main simulation. During spinup, the  
171 coupler repeatedly calls all the model components in their dependency-driven ordering,  
172 using an annual time step. Each component signals whether it needs further steps to  
173 stabilize, and this process repeats until all components signal that they are complete.

174 Currently only the model's carbon cycle makes use of the spinup phase. Spinup  
175 takes place prior to land use change or industrial emission inputs, and the main carbon  
176 cycle moves from its initial, user-defined carbon pool values to a steady state in which  
177  $dC/dt < \epsilon$  for all pools. The convergence criterion  $\epsilon$  is user-definable; by default  $\epsilon = 1 \text{ Tg}$   
178  $\text{C yr}^{-1}$ . From its default values the preindustrial carbon cycle will typically stabilize in 300-  
179 400 time steps.

180 Hector can be forced to match its output to a user-supplied time series. This is  
181 helpful to isolate and test different components. Available constraints currently include  
182 atmospheric  $\text{CO}_2$ , global temperature anomaly, total ocean-atmosphere carbon

183 exchange, total land-atmosphere carbon exchange, and total radiative forcing. Most  
184 constraints operate by overwriting model-calculated values with user-supplied time  
185 series data during the run. The atmospheric [CO<sub>2</sub>] constraint operates slightly  
186 differently, as the global carbon cycle is subject to a continuous mass-balance check. As  
187 a result, when the user supplies a [CO<sub>2</sub>] record between arbitrary dates and orders the  
188 model to match it, the model *computes* [CO<sub>2</sub>] at each time step, and any deficit (surplus)  
189 in comparison with the constraint [CO<sub>2</sub>] is drawn from (added to) the deep ocean. The  
190 deep ocean holds the largest reservoir of carbon; therefore, small changes in this large  
191 pool have a negligible effect on the carbon cycle dynamics. When the model exits the  
192 constraint time period, atmospheric [CO<sub>2</sub>] again becomes fully prognostic.

## 193 **2.5 Code availability and dependencies**

194 All Hector code is open source and available at  
195 <https://github.com/JGCRI/hector/>. The repository includes model code that can be  
196 compiled on Mac, Linux, and Windows, input files for the four Representative  
197 Concentration Pathways (RCP) cases discussed in Section 5, R scripts to process model  
198 output, and extensive documentation. Software dependencies are as limited as possible,  
199 with only the GNU Scientific Library (GSL, Gough, 2009) and the Boost C++ libraries  
200 (<http://www.boost.org>) required. An optional unit testing build target requires the  
201 googletest framework (<http://code.google.com/p/googletest>). However, this is not  
202 needed to compile and run Hector. HTML documentation can be automatically  
203 generated from the code using the Doxygen tool (<http://www.doxygen.org>). All these  
204 tools and libraries are free and open source.

205

### 206 **3.0 Carbon Cycle**

207 In the model's default terrestrial carbon cycle, terrestrial vegetation, detritus,  
208 and soil are linked with each other and the atmosphere by first-order differential  
209 equations (**Figure 2**). Vegetation net primary production is a function of atmospheric  
210 [CO<sub>2</sub>] and temperature. Carbon flows from the vegetation to detritus and then to soil,  
211 losing fractions to heterotrophic respiration on the way. Land-use change emissions are  
212 specified as inputs. An 'earth' pool debits carbon emitted as anthropogenic emissions,  
213 allowing a continual mass-balance check across the entire carbon cycle.

214 More formally, any change in atmospheric carbon, and thus [CO<sub>2</sub>], occurs as a  
215 function of anthropogenic fossil fuel and industrial emissions ( $F_A$ ), land-use change  
216 emissions ( $F_{LC}$ ), and the atmosphere-ocean ( $F_O$ ) and atmosphere-land ( $F_L$ ) carbon fluxes.  
217 The atmosphere is treated as a single well-mixed box whose rate of change is:

$$\frac{dC_{atm}}{dt} = F_A(t) + F_{LC}(t) - F_O(t) - F_L(t) \quad (1)$$

218 Note, that the carbon cycle is solved under indeterminate time steps  
219 (represented in the text by equations with d/dt), while most other submodels of Hector  
220 are solved under a fixed time step of 1 year (equations with  $\Delta$ ). Future versions of  
221 Hector will incorporate indeterminate time steps within all components of the model.  
222 The overall terrestrial carbon balance (Equation 2) excluding user-specified land-use  
223 change fluxes at time  $t$  is the difference between net primary production ( $NPP$ ) and  
224 heterotrophic respiration ( $RH$ ). This is summed over user-specified  $n$  groups (each  
225 typically regarded as a latitude band, biome, or political unit), with  $n \geq 1$ :

$$F_L(t) = \sum_{i=1}^n NPP_i(t) - RH_i(t) \quad (2)$$

226 Note that *NPP* here is assumed to include non-LUC disturbance effects (e.g., fire), for  
 227 which there is currently no separate term. For each biome *i*, *NPP* is computed as a  
 228 function of its preindustrial values *NPP*<sub>0</sub>, current atmospheric carbon *C*<sub>atm</sub>, and the  
 229 biome's temperature anomaly *T*<sub>*i*</sub>, while heterotrophic respiration *RH* depends upon the  
 230 pool sizes of detritus (*C*<sub>d</sub>) and soil (*C*<sub>s</sub>), and global temperatures:

$$NPP_i(t) = NPP_0 * f(C_{atm}, \beta_i) \quad (3)$$

$$f(C_{atm}, \beta_i) = 1 + \beta_i \left( \log \left( \frac{C_{atm}}{C_0} \right) \right) \quad (4)$$

$$RH_{s,d}(t) = C_{s,d} * f_{rs,rd} * Q_{10i}^{T_i(t)/10} \quad (5)$$

$$T_i(t) = T_G(t) * \delta_i \quad (6)$$

231 These are commonly used formulations: *NPP* is modified by a user-specified  
 232 carbon fertilization parameter,  $\beta$  (Piao et al., 2013), that is constant in time but not  
 233 necessarily in space. For example, users can define separate  $\beta$  values for different  
 234 biomes. *RH* changes are controlled by a biome-specific *Q*<sub>10</sub> value. Biomes can  
 235 experience temperature changes at rates that differ from the global mean *T*<sub>G</sub>, controlled  
 236 by a user specified temperature factor  $\delta_i$ . Note that in equation (5), soil *RH* depends on a  
 237 running mean of past temperatures, representing the slower propagation of heat  
 238 through soil strata. Land carbon pools (vegetation, detritus, and soil) change as a result  
 239 of *NPP*, *RH*, and land-use change fluxes, whose effects are partitioned among these  
 240 carbon pools. In addition, carbon flows from vegetation to detritus and to soil (**Figure 2**).  
 241 Partitioning fractions (*f*) control the flux quantities between pools (**Table 2**). For

242 simplicity Equations 7-9 omit the time  $t$  and biome-specific  $i$  notations, but each pool is  
 243 tracked separately for each biome at each time step:

$$\frac{dC_V}{dt} = NPP f_{nv} - C_V(f_{vd} + f_{vs}) - F_{LC} f_{lv} \quad (7)$$

$$\frac{dC_D}{dt} = NPP f_{nd} + C_V f_{vd} - C_D f_{ds} - RH_{det} - F_{LC} f_{ld} \quad (8)$$

$$\frac{dC_S}{dt} = NPP f_{ns} + C_V f_{vs} + C_D f_{ds} - RH_{soil} - F_{LC} f_{ls} \quad (9)$$

244 The ocean-atmosphere carbon flux is the sum of the ocean's surface fluxes ( $F_i$ )  
 245 (currently  $n=2$ , high and low latitude surface box):

$$F_O(t) = \sum_{i=1}^n F_i(t) \quad (10)$$

246 The surface fluxes of each individual box are directly calculated from an ocean chemistry  
 247 submodel described in detail by Hartin et al. (in prep). We model the nonlinearity of the  
 248 inorganic carbon cycle, calculating  $pCO_2$ , pH, and carbonate saturations based on  
 249 equations from Zeebe and Wolf-Gladrow, (2001). The flux of  $CO_2$  for each box  $i$  is  
 250 calculated by:

$$F_i(t) = k \alpha \Delta pCO_2 \quad (11)$$

251 where  $k$  is the  $CO_2$  gas-transfer velocity,  $\alpha$  is the solubility of  $CO_2$  in water based on  
 252 salinity, temperature, and pressure, and  $\Delta pCO_2$  is the atmosphere-ocean gradient of  
 253  $pCO_2$  (Takahashi et al., 2009). The calculation of  $pCO_2$  in each surface box is based on  
 254 the concentration of  $CO_2$  in the ocean and its solubility (a function of temperature,  
 255 salinity, and pressure). At steady state, the cold high latitude surface box ( $>55^\circ$ , subpolar  
 256 gyres) acts as a sink of carbon from the atmosphere, while the warm low latitude

257 surface box (<55°) off gases carbon back to the atmosphere. Temperatures of the  
 258 surface boxes are linearly related to atmospheric global temperatures (see section 4.1),  
 259  $T_{HL} = \Delta T - 13$  and  $T_{LL} = \Delta T + 7$  (Lenton, 2000). The ocean model, modeled after Lenton et  
 260 al. (2000) and Knox and McElroy (1984), circulates carbon through four boxes (two  
 261 surface, one intermediate depth, one deep), via water mass advection and exchange,  
 262 simulating a simple thermohaline circulation (**Figure 2**). At steady state, approximately  
 263 100Pg of carbon are transferred from the high latitude surface box to the deep box  
 264 based on the volume of the box and transport in Sv ( $10^6 \text{ m}^3 \text{ s}^{-1}$ ) between the boxes. The  
 265 change in carbon of any box  $i$  is given by the fluxes in and out, with  $F_{atm \rightarrow i}$  as the  
 266 atmosphere-ocean carbon flux:

$$\frac{dC_i}{dt} = \sum_{j=1}^{in} F_{j \rightarrow i} - \sum_{j=1}^{out} F_{i \rightarrow j} + F_{atm \rightarrow i} \quad (12)$$

267 As the model advances, the carbon in PgC is converted to dissolved inorganic carbon  
 268 (DIC) in each box. The new DIC values are used within the chemistry submodel to  
 269 calculate  $p\text{CO}_2$  values at the next time step.

### 270 **3.1 Adaptive-time step solver**

271 The fundamental time step in Hector is currently one year, and most model  
 272 components are solved at this resolution. The carbon cycle, however, operates on a  
 273 variable time step, ensuring accurate ODE solutions, even under high-emissions  
 274 scenarios. This will also allow future sub-annual applications where desired. The  
 275 adaptive time step accomplished using the *gsl\_odeiv2\_evolve\_apply* solver package of  
 276 GSL 1.16, which varies the time step to keep truncation error within a specific tolerance

277 when advancing the model. Thus all the carbon cycle components handle indeterminate  
278 time steps less than or equal to 1 year, and can signal the solver if a too-large time step  
279 is leading to instability. The solver then re-retries the solution, using a series of smaller  
280 steps. From the coupler’s point of view, however, the entire model continues to  
281 advance in annual increments.

## 282 **4.0 Other Components**

### 283 **4.1 Global Atmospheric Temperature**

284 Near surface global atmospheric temperature is calculated by:

$$\Delta T(t) = \lambda * RF(t) - F_H(t) \quad (13)$$

285 where the user-specified  $\lambda$  is the climate feedback parameter, defined as  $\lambda = S'/S$ ,  $S'$  is  
286 the climate sensitivity parameter (3 K) and  $S$  is the equilibrium climate sensitivity for a  
287 doubling of  $\text{CO}_2$  ( $3.7 \text{ W m}^{-2}$ ) (Knutti and Hegerl, 2008).  $RF$  is the total radiative forcing  
288 and  $F_H$  is the ocean heat flux.  $F_H$  is calculated by a simple sigmoidal expression of the  
289 ocean heat uptake efficiency  $k$  ( $\text{W m}^{-2} \text{ K}^{-1}$ ) that decreases with increasing global  
290 temperatures) multiplied by the atmospheric temperature change prior to the ocean’s  
291 removal of heat from the atmosphere ( $T_H$ ) (Raper et al., 2002).

$$\Delta F_H(t) = k * \Delta T_H(t) \quad (14)$$

292 As global temperatures rise, the uptake capacity of the ocean may diminish, simulating  
293 both a saturation of heat in the surface and a slowdown in ocean circulation with  
294 increased temperatures. Finally, the temperature effects from atmospheric  $[\text{CO}_2]$  are

295 lagged in time, as there are numerous real-world processes not simulated in Hector  
296 buffering the temperature effects of increasing atmospheric [CO<sub>2</sub>].

## 297 **4.2 Radiative Forcing**

298 Radiative forcing is calculated from a series of atmospheric greenhouse gases,  
299 aerosols, and pollutants (**Eq. 15-16, 18-22, 25, 29-30**). Radiative forcing is reported as  
300 the relative radiative forcing. The base year user-specified forcings are subtracted from  
301 the total radiative forcing to yield a forcing relative to the base year (1750).

### 302 **4.2.1. CO<sub>2</sub>**

303 Radiative forcing from atmospheric [CO<sub>2</sub>] in W m<sup>-2</sup> is calculated based on  
304 Meinshausen et al. (2011a):

$$RF_{CO_2} = 5.35 * \log \frac{Ca}{C0} \quad (15)$$

305 where, 5.35 W m<sup>-2</sup> is a scaling parameter from Myhre et al. (1998), *Ca* is the  
306 current atmospheric [CO<sub>2</sub>] in ppmv and *C0* is the preindustrial [CO<sub>2</sub>] in ppmv.

### 307 **4.2.2 Halocarbons**

308 The halocarbon component of the model can accept an arbitrary number of gas  
309 species, each characterized by a name, a lifetime  $\tau$  (yr), a radiative forcing efficiency  $\alpha$   
310 (W m<sup>-2</sup> pptv<sup>-1</sup>), an optional user-specified preindustrial concentration (pptv), and a  
311 molar mass (g). For each gas, its concentration (*C<sub>i</sub>*) at time *t* is then computed based on  
312 a specified emissions time series *E*, assuming an exponential decay from the  
313 atmosphere:

$$C(t) = C_0 * \exp\left(-\frac{t}{\tau}\right) + E * \tau * \left(1 - \exp\left(-\frac{t}{\tau}\right)\right) \quad (16)$$



315 E is corrected for atmospheric dry air mole constant (1.8) and the molar mass of each  
316 halocarbon. The default model input files include these parameters and a time series of  
317 emissions for C2F6, CCl4, CF4, CFC11, CFC12, CFC113, CFC114, CFC115, CH3Br, CH3CCl3,  
318 CH3Cl, HCF22, HCF141b, HCF142b, HFC23, HFC32, HFC125, HFC134a, HFC143a,  
319 HFC227ea, HFC245ca, HFC245fa, HFC4310, SF6, halon1211, halon1301, and halon2402.

320 Radiative forcing by halocarbons, and other gases controlled under the Montreal  
321 Protocol, SF<sub>6</sub>, and ozone are calculated via:

$$RF = \alpha [ C(t) ] \quad (17)$$

322 where  $\alpha$  is the radiative efficiency (input parameters) in W m<sup>-2</sup> ppbv<sup>-1</sup>, and C is the  
323 atmospheric concentration.

#### 324 **4.2.3 Ozone**

325 Tropospheric ozone concentrations are calculated from the CH<sub>4</sub> concentration  
326 and the emissions of three primary pollutants: NO<sub>x</sub>, CO, and NMVOCs, modified from  
327 Tanaka et al. (2007a):

$$O_{3_t} = (5.0 * \ln[CH_4]) + (0.125 * ENO_x) + (0.0011 * ECO) \quad (18) \\ + (0.0033 * EVOC)$$

328 where the constants are the ozone sensitivity factors for each of the precursors (Ehhalt  
329 et al., 2001). The radiative forcing of tropospheric ozone is calculated from a linear  
330 relationship using a radiative efficiency factor (Joos et al., 2001a):

$$RF_{O_3} = 0.042 * [O_3] \quad (19)$$

333

#### 4.2.4 BC and OC

334 The radiative forcing from black and organic carbon is a function their emissions (*EBC*  
335 and *EOC*).

$$RF_{BC} = 0.0743 \text{ Wm}^{-2}\text{Tg}^{-1} * EBC \quad (20)$$

$$RF_{OC} = -0.0128 \text{ Wm}^{-2}\text{Tg}^{-1} * EOC \quad (21)$$

336 The coefficients include both indirect and direct forcings of black and organic carbon  
337 (fossil fuel and biomass) (Bond et al., 2013, table C1).

338

#### 4.2.5 Sulphate Aerosols

339 The radiative forcing from sulphate aerosols is a combination of the direct and indirect  
340 forcings (Joos et al., 2001a).

$$RF_{SOx \text{ Direct}} = -0.35 \text{ Wm}^{-2} * \frac{ESO_{xt}}{ESO_{xt0}} \quad (22)$$

$$RF_{SOx \text{ Indirect}} = -0.6 \text{ Wm}^{-2} * \frac{(\ln(ESN) + EeSO_{xt})}{ESN} \quad (23)$$
$$* \left( \ln \frac{ESN + EeSO_{xt0}}{ESN} \right)^{-1}$$

341 The direct forcing by sulphate aerosols is proportional to the anthropogenic sulphur  
342 emissions ( $\text{GgS yr}^{-1}$ ) divided by the sulphate emissions from 2000. The indirect forcing by  
343 sulphate aerosols is a function of the anthropogenic and natural sulphur emissions.

344 Natural sulphur emissions, denoted by *ESN*, are equal to 42000 Gg S. A time series of  
345 annual mean volcanic stratospheric aerosol forcing ( $\text{W m}^{-2}$ ) is supplied from  
346 Meinshausen et al. (2011b) and added to the indirect and direct forcing for a total  
347 sulphate forcing.

348

#### 4.2.6 Methane (CH<sub>4</sub>)

349 The change in [CH<sub>4</sub>] is calculated directly from CH<sub>4</sub> emissions, and sinks of CH<sub>4</sub> in the the  
 350 troposphere (based on the lifetime of OH), stratosphere, and soil based on Wigley et al.  
 351 (2002).

$$\Delta CH_4 = \frac{E(CH_4)}{2.78} - \frac{[CH_4]}{T_{OH}} - \frac{[CH_4]}{T_{strat}} - \frac{[CH_4]}{T_{soil}} \quad (24)$$

352 where E is total CH<sub>4</sub> emissions (Tg yr<sup>-1</sup>) from both natural and anthropogenic sources,  
 353 2.78 (Tg ppb<sup>-1</sup>) is the conversion factor, and T are the lifetimes of the tropospheric sink  
 354 (T<sub>OH</sub>), the stratospheric sink (T<sub>strat</sub> = 120 year), and the soil sink (T<sub>soil</sub> = 160 year). Note  
 355 that within Hector, natural emissions are held at a constant 300 Tg yr<sup>-1</sup>.

356 The lifetime of OH is a function of [CH<sub>4</sub>], and the emissions of NO<sub>x</sub>, CO and VOC,  
 357 based on Tanaka et al. (2007a).

$$\begin{aligned} \ln(OH)_t = & -0.32 (\ln[CH_4]_t - \ln[CH_4]_{t_0}) + 0.0042 (E(NO_x)_t - (E(NO_x)_{t_0})) \\ & - 0.000105 (E(CO)_t - (E(CO)_{t_0})) \\ & - 0.00315 (E(VOC)_t - (E(VOC)_{t_0})) \end{aligned} \quad (25)$$

358 The radiative forcing equation for CH<sub>4</sub> (Joos et al., 2001a) is a function of the  
 359 concentrations (ppbv) of both CH<sub>4</sub> and N<sub>2</sub>O:

$$\begin{aligned} RF_{CH_4} = & 0.036 \text{ Wm}^{-2} \left[ \sqrt{[CH_4](t)} - \sqrt{[CH_4](t_0)} \right] \\ & - f[CH_4(t), N_2O(t_0)] - f[CH_4(t_0), N_2O(t_0)] \end{aligned} \quad (26)$$

360 The function *f* accounts for the overlap in CH<sub>4</sub> and N<sub>2</sub>O in their bands is:

$$f(M, N) = 0.47 \quad (27)$$

$$\begin{aligned} & * \ln(1 + (2.01 * 10^{-5}) * (MN)^{0.75} + (5.31 * 10^{-15}) * M \\ & * (MN)^{1.52}) \end{aligned}$$

361 **4.2.7 N<sub>2</sub>O**

362 The change in [N<sub>2</sub>O] is a function of N<sub>2</sub>O emissions, and the lifetime of N<sub>2</sub>O based on

363 Ward and Mahowald (2014).

$$\Delta N_{2O} = \frac{E(N_{2O})}{4.8} - \frac{[N_{2O}]}{\tau_{N_{2O}}} \quad (28)$$

364 where E is total N<sub>2</sub>O emissions (Tg N yr<sup>-1</sup>), both natural and anthropogenic, 4.8 (Tg N

365 ppbv<sup>-1</sup>) is the conversion factor, and τ<sub>N<sub>2</sub>O</sub> is the lifetime of N<sub>2</sub>O. We set natural

366 emissions of N<sub>2</sub>O to linearly decrease from 11 Tg N yr<sup>-1</sup> in 1765, to 8 Tg N yr<sup>-1</sup> in 2000

367 and are then held constant at 8 Tg N yr<sup>-1</sup> to 2300. The lifetime of N<sub>2</sub>O is a function of its

368 initial lifetime (τ<sub>0</sub>) and concentration ([N<sub>2</sub>O]<sub>t0</sub>).

$$\tau_{N_{2O}} = \tau_0 * \left( \frac{[N_{2O}]_t}{[N_{2O}]_{t0}} \right)^{-0.05} \quad (29)$$

369 The radiative forcing equation for N<sub>2</sub>O (Joos et al., 2001a) is a function of the

370 concentration (ppbv) of both CH<sub>4</sub> and N<sub>2</sub>O:

$$\begin{aligned} RF_{N_{2O}} = 0.12 \text{ Wm}^{-2} & \left[ \sqrt{[N_{2O}]_t} - \sqrt{[N_{2O}]_{t0}} \right] - f[CH_4(t_0), N_{2O}(t)] \\ & - f[CH_4(t_0), N_{2O}(t_0)] \end{aligned} \quad (30)$$

371 The function *f* accounts for the overlap in CH<sub>4</sub> and N<sub>2</sub>O in their bands is the same as

372 equation 27.

373

#### 4.2.8 Stratospheric H<sub>2</sub>O from CH<sub>4</sub> oxidation:

374 The radiative forcing from stratospheric H<sub>2</sub>O is a function of the [CH<sub>4</sub>] (Tanaka et al.,  
375 2007a). The coefficient 0.05 is from Joos et al. (2001a) based on the fact that the forcing  
376 contribution from stratospheric H<sub>2</sub>O is about 5% of the total CH<sub>4</sub> forcing (IPCC, 2001).  
377 The 0.036 value of the coefficient corresponds to the same value used in the CH<sub>4</sub>  
378 radiative forcing equation.

$$RF_{stratH2O} = 0.05 * \left\{ 0.036 \text{ Wm}^{-2} * \left( \sqrt{[CH_4]_t} - \sqrt{[CH_4]_{t0}} \right) \right\} \quad (31)$$

379

#### 380 5.0 Model Experiments and Data Sources

381 A critical test of Hector's performance is to compare the major climatic variables  
382 calculated in Hector, e.g., atmospheric [CO<sub>2</sub>], radiative forcing, and atmospheric  
383 temperature, to observational records and both simple and complex climate models.  
384 Within this study, Hector is run under prescribed emissions from 1850 to 2300 for all  
385 four Representative Concentration Pathways (RCPs), freely available at  
386 <http://tntcat.iiasa.ac.at/RcpDb/> (Moss et al., 2010; van Vuuren et al., 2007; Clarke et al.,  
387 2007; Wise et al., 2009; Riahi et al., 2007; Fujino et al., 2006; Hijioka et al., 2008; Smith  
388 and Wigley, 2006). The RCPs are plausible future scenarios that were developed to  
389 improve our understanding of the coupled human climate system. RCPs by definition  
390 are concentration pathways; however, for all experiments within this manuscript we use  
391 the corresponding emissions trajectories from each RCP as input for Hector.

392 Comparison data was obtained from a series of models. We compared Hector  
393 results to MAGICC, a SCM widely used in the scientific and IAM communities, for global

394 variables such as atmospheric CO<sub>2</sub>, radiative forcing, and temperature (e.g., Raper et al.,  
395 2001; Wigley, 1995; Meinshausen et al., 2011a). We also compare Hector to a suite of  
396 eleven Earth System Models included in the 5<sup>th</sup> Coupled Model Intercomparison Project  
397 (CMIP5) archive (Taylor et al., 2012) (**Table 3**). All CMIP5 data were converted to yearly  
398 global averages from the historical period through the RCPs and their extensions. One  
399 standard deviation of the annual global averages and the CMIP5 model range were  
400 calculated for each variable using the RCMIP5 (<http://github.com/JGCRI/RCMIP5>)  
401 package in R. All CMIP5 variables used in this study are from model runs with  
402 prescribed atmospheric concentrations, except for comparisons involving atmospheric  
403 [CO<sub>2</sub>] which are from the emissions driven scenario (esmHistorical and esmRCP8.5)  
404 (Figures 3 and 5). We acknowledge that this comparison, between an emissions-forced  
405 model (Hector) and concentration-forced models (CMIP5), is not perfect. However, very  
406 few CMIP5 models were run under prescribed emissions scenarios.

407         We compare Hector to observations of atmospheric [CO<sub>2</sub>] from Law Dome  
408 (1010-1975) and Mauna Loa (1958 – 2008), (Keeling and Whorf, 2005; Etheridge et al.,  
409 1996) . Global temperature anomalies are from HadCRUT4 (Morice et al., 2012).  
410 Observations of air-sea and air-land fluxes are from the Global Carbon Project (GCP) (Le  
411 Quéré et al., 2013). Lastly, observations of surface ocean pH are from Bermuda Atlantic  
412 Time Series (BATS) and Hawaii Ocean Time Series (HOTS) (Bates, 2007; Fujieki et al.,  
413 2013).

414

## 415 **6.0 Results and Discussion**

### 416 **6.1 Historical**

417 A critical test of Hector's performance is how well it compares to historical and  
418 present day climate from observations, MAGICC, and a suite of CMIP5 models. Delta  
419 changes and root mean square errors were calculated for Hector's primary outputs,  
420 which are summarized in **Table 4**. After spinup is complete in Hector, atmospheric [CO<sub>2</sub>]  
421 in 1850 is 286.0 ppmv, which compares well with observations from Law Dome of 285.2  
422 ppmv. Hector captures the global trends in atmospheric [CO<sub>2</sub>] (**Figure 3**) with an  
423 average root mean square error (RMSE) of 2.85 ppmv (**Table 4a**), when compared to  
424 observations, MAGICC6, and CMIP5 data from 1850-2005. Delta change of atmospheric  
425 [CO<sub>2</sub>] from 1850-2005 is slightly lower than the observations, MAGICC6, and CMIP5.  
426 Hector can be forced to match atmospheric [CO<sub>2</sub>] records (section 2.4), but we disabled  
427 this feature to highlight the full performance of the model. Note however, that in the  
428 MAGICC6 results a similar feature was used to force the output to match the historical  
429 atmospheric [CO<sub>2</sub>] record.

430 Historical global atmospheric temperature anomalies (relative to 1850) are  
431 compared across Hector, MAGICC6, CMIP5, and observations from HadCRUT4 (**Figure**  
432 **4**). Atmospheric temperature change from Hector (0.98 °C) over the period 1850 to  
433 2005 closely match the CMIP5 temperature change (1.01 °C), both slightly higher than  
434 the observational record. Over this time period a Hector has an average RMSE of 0.14  
435 °C. Note that simple climate models do not aim to capture temperature variations due

436 to interannual/decadal variability found in ESMs or the real world; instead they simulate  
437 the overall trends in global mean temperature change.

## 438 **6.2 Future Projections**

439 Hector's strengths lie within policy relevant time scales of decades to centuries,  
440 and here we compare Hector to MAGICC and CMIP5 under differing future climate  
441 projections. Results from all four RCPs are broadly similar when comparing Hector, to  
442 MAGICC6, and CMIP5; we display here RCP8.5 results as representative. Studies suggest  
443 that 80% of the anthropogenic CO<sub>2</sub> emissions have an average atmospheric lifetime of  
444 300-450 years (Archer et al., 1997; Rogner, 1997; Archer, 2005). Hector has all the  
445 necessary components to model the climate system from present day through the next  
446 approximately 300 years. **Figure 5** highlights historical trends in atmospheric [CO<sub>2</sub>],  
447 along with projections of atmospheric [CO<sub>2</sub>] under esmRCP8.5 from 1850 to 2100. Note  
448 that the emissions forced scenario only extends to 2100 and not to 2300 like the  
449 concentration forced scenarios (e.g., Figure 8). Both Hector and MAGICC6 are on the  
450 low end of the CMIP5 median, but fall within one standard deviation and model range,  
451 with a RMSE of 9.0 ppmv (**Table 4b**).

452 The CMIP5 archive does not provide emissions prescribed scenarios for all RCPs;  
453 we can only compare atmospheric [CO<sub>2</sub>] from Hector with MAGICC6 under all four RCP  
454 scenarios out to 2300 (**Figure 6**). Hector's change in [CO<sub>2</sub>] (1472.13 ppmv) from 1850 to  
455 2300 is slightly lower than MAGICC6 (1600.0 ppmv) for RCP 8.5. This is most likely due  
456 to different representations of the global carbon cycle. We compare Hector to  
457 MAGICC6 for changes in radiative forcing under the four RCPs (**Figure 7**). Radiative



458 forcing was not provided within the CMIP5 archive and therefore we can only compare  
459 Hector and MAGICC6. Over the period 1850 to 2300 Hector ( $12.80 \text{ Wm}^{-2}$ ) and MAGICC6  
460 ( $12.24 \text{ Wm}^{-2}$ ) are comparable in their change in radiative forcing, with a RMSE of  $0.26 \text{ W}$   
461  $\text{m}^{-2}$ . One noticeable difference between MAGICC6 and Hector during the historical  
462 period is the decreases in radiative forcing. This is due to the effects of volcanic  
463 emissions on radiative forcing. For simplicity, we have chosen to run Hector without  
464 these effects.

465 **Figure 8** compares global temperature anomalies from Hector to MAGICC6 and  
466 CMIP5 over the four RCPs, from 2005 to 2300. Hector simulates the CMIP5 median  
467 more closely than MAGICC6 across all four RCPs, with a temperature change under RCP  
468 8.5 for Hector of  $8.59 \text{ }^\circ\text{C}$ , compared to MAGICC6 of  $7.30 \text{ }^\circ\text{C}$ , while the temperature  
469 change for CMIP5 is  $9.57 \text{ }^\circ\text{C}$  (**Table 4c**). To highlight this close comparison, temperature  
470 change over the entire record (1850-2300) for Hector is  $9.58 \text{ }^\circ\text{C}$ , which is within  $1.0 \text{ }^\circ\text{C}$  of  
471 the CMIP5 median, while MAGICC6's temperature change is greater than  $2.5 \text{ }^\circ\text{C}$  away  
472 from the CMIP5 median.

473 **Figures 9 and 10** present a detailed view of carbon fluxes under RCP 8.5, for  
474 CMIP5 and observations (negative represents carbon flux to the atmosphere). The  
475 ocean is a major sink of carbon through 2100, becoming less effective with time in both  
476 Hector and the CMIP5 models. MAGICC6 does not include air-sea fluxes in its output,  
477 and because it is not open source we were unable to obtain these values. Therefore, we  
478 compare air-sea fluxes of  $\text{CO}_2$  to MAGICC5.3, updated with explicit BC and OC forcing as  
479 described in Smith and Bond (2014). Hector's calculation of air-sea fluxes is within the

480 large CMIP5 model range up to 2100. However, after that Hector peaks close to 2150,  
481 while the CMIP5 models are beginning to decline. One potential reason for this  
482 discrepancy after 2100 is that in this version of Hector, we do not simulate changes in  
483 ocean circulation, potentially biasing fluxes too high after 2100. Most ESMs in CMIP5  
484 show a weakening of the Atlantic meridional overturning circulation by 2100 between  
485 15% and 60% under RCP 8.5 (Cheng et al., 2013). A slowdown in ocean circulation may  
486 result in less carbon uptake by the oceans. Another potential reason for this bias is  
487 Hector's constant pole to equator ocean temperature gradient. Studies show that the  
488 Arctic is warming faster than the rest of the globe (e.g., Bintanja and van der Linden,  
489 2013; Holland and Bitz, 2003; Bekryaev et al., 2010). A warmer high latitude surface  
490 ocean in Hector would suppress the uptake of carbon, potentially bringing the air-sea  
491 fluxes closer to the CMIP5 median after 2100.

492 CMIP models tend to show huge divergences in their land responses to changing  
493 climate (e.g., Friedlingstein et al., 2006), which is evident by the large range in CMIP5  
494 models (**Figure 10**). Hector simulates the general trends, of increasing carbon sink and  
495 then a gradual decline to a carbon source after 2100. Both land and ocean fluxes within  
496 Hector agree well the observations from Le Queré et al., (2013).

497 One feature in Hector that is unique amongst SCMs is its ability to actively solve  
498 the carbonate system in the upper ocean (Hartin et al, in prep). This feature allows us  
499 to predict changes ocean acidification, calcium carbonate saturations and other  
500 carbonate system parameters. **Figure 11** shows low latitude (<55°) pH for Hector  
501 compared to CMIP5 and observations from 1850 to 2100 under RCP 8.5. The model

502 projects a significant drop in pH from present day through 2100, which may lead to  
503 detrimental effects on marine ecosystems (e.g., Fabry et al., 2008).

504

## 505 **7.0 Conclusions**

506 Hector reproduces the large-scale couplings and feedbacks on the climate  
507 system between the atmosphere, ocean, and land, falling within the range of the CMIP5  
508 model and matching MAGICC. It does not simulate the fine details or parameterizations  
509 found in large-scale, complex ESMs, but instead represents the most critical global  
510 processes in a reduced-complexity form. This allows for fast execution times, ease of  
511 understanding, and straightforward analysis of the model output.

512 Two of Hector's key features are its open source nature and modular design.  
513 This allows the user to edit the input files and code at will, for example to  
514 enable/disable/replace components, or include components not found within the core  
515 version of Hector. For example, a user can design a new submodel (e.g., sea-ice) to  
516 answer specific climate questions relating to that process. Hector is hosted on a widely-  
517 used open source software repository (Github), and thus changes and improvements  
518 can be easily shared with the scientific community. Because of these critical features,  
519 Hector has the potential to be a key analytical tool in both the policy and scientific  
520 communities. We welcome user input and encourage use, modifications, and  
521 collaborations with Hector.

522 While Hector has many strengths, the current 1.0 version has some limitations.  
523 For example, Hector does not currently simulate terrestrial gross primary production, a

524 key metric of comparison to e.g. the FLUXNET database. Also, Hector does not have  
525 differential radiative forcing and atmospheric temperature calculations over land and  
526 ocean. This may be a problem, as land responds to changes in emissions of greenhouse  
527 gases, and aerosols much quicker than the ocean (Hansen et al., 2005). Hector does not  
528 explicitly deal with oceanic heat uptake, except via a simple empirical formula. Surface  
529 temperatures are calculated based on a linear relationship with atmospheric  
530 temperature and we assume a constant pole to equator temperature gradient. We  
531 acknowledge that this assumption may not hold true if the poles warm faster than the  
532 equator.

533 Future plans with Hector include addressing some of the above limitations and  
534 conducting numerous scientific experiments, using Hector as a stand-alone simple  
535 climate carbon-cycle model. It is also being incorporated into Pacific Northwest  
536 National Laboratory's Global Change Assessment Model for policy-relevant experiments.  
537 Hector has the ability to be a key analytical tool used across many scientific and policy  
538 communities due to its modern software architecture, open source, and object-oriented  
539 structure.

540

#### 541 **Code Availability**

542 Hector is freely available at <https://github.com/JGCRI/hector> . The specific Hector v1.0  
543 referenced in this paper, as well as code to reproduce all figures and results shown here,  
544 is available at <https://github.com/JGCRI/hector/releases/tag/v1.0>

#### 545 **Author contributions**

546 C.A.H. and B.P.B.-L. developed the ocean and terrestrial carbon models, respectively,  
547 and led the overall development of Hector. R.P.L. and P.P. wrote critical code for  
548 Hector's coupler and carbon cycle solver. A.S. helped with the development of the  
549 atmospheric forcing components. C.A.H. wrote the manuscript with contributions from  
550 all co-authors.

551

## 552 **Acknowledgements**

553 This research is based on work supported by the U.S. Department of Energy, Office of  
554 Science, Integrated Assessment Research Program. The Pacific Northwest National  
555 Laboratory is operated for DOE by Battelle Memorial Institute under contract DE-AC05-  
556 76RL01830.

557 **References:**

- 558 Anthoff, D., and Tol, R. S. J.: The income elasticity of the impact of climate change, Is  
559 the Environment a Luxury? An inquiry into the relationship between environment and  
560 income, edited by: Tiezzi, S., and Martini, C., Routledge, 2014.
- 561 Applegate, P. J., Kirchner, N., Stone, E. J., Keller, K., and Greve, R.: An assessment of  
562 key model parametric uncertainties in projections of Greenland Ice Sheet behavior, *The*  
563 *Cryosphere*, 6, 589-606, 10.5194/tc-6-589-2012, 2012.
- 564 Archer, D., Kheshgi, H., and Maier-Reimer, E.: Multiple timescales for neutralization of  
565 fossil fuel CO<sub>2</sub>, *Geophysical Research Letters*, 24, 405-408, 10.1029/97GL00168, 1997.
- 566 Archer, D.: Fate of fossil fuel CO<sub>2</sub> in geologic time, *Journal of Geophysical Research:*  
567 *Oceans*, 110, C09S05, 10.1029/2004JC002625, 2005.
- 568 Bates, N. R.: Interannual variability of the oceanic CO<sub>2</sub> sink in the subtropical gyre of the  
569 North Atlantic Ocean over the last 2 decades, *Journal of Geophysical Research: Oceans*,  
570 112, C09013, 10.1029/2006JC003759, 2007.
- 571 Bekryaev, R. V., Polyakov, I. V., and Alexeev, V. A.: Role of Polar Amplification in  
572 Long-Term Surface Air Temperature Variations and Modern Arctic Warming, *Journal of*  
573 *Climate*, 23, 3888-3906, 10.1175/2010JCLI3297.1, 2010.
- 574 Bintanja, R., and van der Linden, E. C.: The changing seasonal climate in the Arctic, *Sci.*  
575 *Rep.*, 3,  
576 [http://www.nature.com/srep/2013/130327/srep01556/abs/srep01556.html#supplementary](http://www.nature.com/srep/2013/130327/srep01556/abs/srep01556.html#supplementary-information)  
577 [-information](http://www.nature.com/srep/2013/130327/srep01556/abs/srep01556.html#supplementary-information), 2013.
- 578 Bond-Lamberty, B., Calvin, K., Jones, A. D., Mao, J., Patel, P., Shi, X., Thomson, A.,  
579 Thornton, P., and Zhou, Y.: Coupling earth system and integrated assessment models: the  
580 problem of steady state, *Geosci. Model Dev. Discuss.*, 7, 1499-1524, 10.5194/gmdd-7-  
581 1499-2014, 2014.
- 582 Bond, T. C., Doherty, S. J., Fahey, D. W., Forster, P. M., Berntsen, T., DeAngelo, B. J.,  
583 Flanner, M. G., Ghan, S., Kärcher, B., Koch, D., Kinne, S., Kondo, Y., Quinn, P. K.,  
584 Sarofim, M. C., Schultz, M. G., Schulz, M., Venkataraman, C., Zhang, H., Zhang, S.,  
585 Bellouin, N., Guttikunda, S. K., Hopke, P. K., Jacobson, M. Z., Kaiser, J. W., Klimont,  
586 Z., Lohmann, U., Schwarz, J. P., Shindell, D., Storelvmo, T., Warren, S. G., and Zender,  
587 C. S.: Bounding the role of black carbon in the climate system: A scientific assessment,  
588 *Journal of Geophysical Research: Atmospheres*, 118, 5380-5552, 10.1002/jgrd.50171,  
589 2013.
- 590 Bouwman, A. F., Hoek, K. W. v. d., Drecht, G. V., and Eickhout, B.: World Livestock  
591 and crop production systems, land use and environment between 1970 and 2030, *Rural*  
592 *Lands, Africulture and Climate beyond 2015: A new prespective on suture land use*  
593 *patterns*, edited by: Brouwer, F., and McCarl, B., Springer, Dordrecht, 2006.
- 594 Calvin, K., Clarke, L., Edmonds, J., Eom, J., Hejazi, M., Kim, S., Kyle, G., Link, R.,  
595 Patel, P., Smith, S., and Wise, M.: GCAM Wiki Documentation, PNNL-20809, Pacific  
596 Northwest National Laboratory, Richland WA, 2011.
- 597 Castruccio, S., McInerney, D. J., Stein, M. L., Crouch, F. L., Jacob, R. L., and Moyer, E.  
598 J.: Statistical Emulation of Climate Model Projections Based on Precomputed GCM  
599 Runs, *Journal of Climate*, 27, 2014.

600 Challenor, P.: Using emulators to estimate uncertainty in complex models, *Uncertainty*  
601 *Quantification in Scientific Computing*, edited by: Dienstry, A. M., and Boisvert, R. F.,  
602 Springer, IFIP AICT 377, 151-164 pp., 2012.

603 Cheng, W., Chiang, J. C. H., and Zhang, D.: Atlantic Meridional Overturning Circulation  
604 (AMOC) in CMIP5 Models: RCP and Historical Simulations, *Journal of Climate*, 26,  
605 7187-7197, 10.1175/JCLI-D-12-00496.1, 2013.

606 Clarke, L., J. Edmonds, H. Jacoby, H. Pitcher, Reilly, J., and Richels, R.: Scenarios of  
607 Greenhouse Gas Emissions and Atmospheric Concentrations. Sub-report 2.1A of  
608 Synthesis and Assessment Product 2.1, edited by: Research, U. S. C. C. S. P. a. t. S. o. G.  
609 C., Department of Energy, Office of Biological & Environmental Research, Washington,  
610 7 DC., USA, 2007.

611 Collins, W. D., Craig, A. P., Truesdale, J. E., Di Vittorio, A. V., Jones, A. D., Bond-  
612 Lamberty, B., Calvin, K. V., Edmonds, J. A., Kim, S. H., Thomson, A. M., Patel, P.,  
613 Zhou, Y., Mao, J., Shi, X., Thornton, P. E., Chini, L. P., and Hurtt, G. C.: The integrated  
614 Earth System Model (iESM): formulation and functionality, *Geosci. Model Dev.*  
615 *Discuss.*, 8, 381-427, 10.5194/gmdd-8-381-2015, 2015.

616 Denman, K. L., G. Brasseur, A. Chidthaisong, P. Ciais, P.M. Cox, R.E. Dickinson, D.  
617 Hauglustaine, C. Heinze, E. Holland, D. Jacob, U. Lohmann, S Ramachandran, P.L. da  
618 Silva Dias, S.C. Wofsy and X. Zhang: *Climat Change 2007: The Physical Science Basis.*,  
619 edited by: Change, C. o. W. G. I. t. t. F. A. R. o. t. I. P. o. C., Cambridge University  
620 Press, Cambridge , United Kingdom and New York, USA, 2007.

621 Di Vittorio, A. V., Chini, L. P., Bond-Lamberty, B., Mao, J., Shi, X., Truesdale, J., Craig,  
622 A., Calvin, K., Jones, A., Collins, W. D., Edmonds, J., Hurtt, G. C., Thornton, P., and  
623 Thomson, A.: From land use to land cover: restoring the afforestation signal in a coupled  
624 integrated assessment–earth system model and the implications for CMIP5 RCP  
625 simulations, *Biogeosciences*, 11, 6435-6450, 10.5194/bg-11-6435-2014, 2014.

626 E.P. White, E. B., Z.T. Brym, K.J. Locey, D.J. McGlenn: Nine simple ways to make it  
627 easier to (re)use your data, *PeerJ PrePrints*, 1:e7v2,  
628 <http://dx.doi.org/10.7287/peerj.preprints.7v2>, 2013.

629 Edmonds, J., and Smith, S. J.: *The Technology of Two Degrees. Avoiding Dangerous*  
630 *Climate Change*, edited by: Schellnhuber, H. J., Cramer, W., Nakicenovic, N., Wigley,  
631 T., and Yohe, G., Cambridge University Press, Cambridge, UK, 2006.

632 Ehhalt, D., Prather, M. J., Dentener, F. J., Derwent, R., Dlugokencky, E. J., Holland, E.  
633 A., Isaksen, I. S., Katima, J., Kirchoff, V., Matson, P. A., and Wang, M.: Atmospheric  
634 chemistry and greenhouse gases, in: *Climate Change 2001: The Scientific Basis*, edited  
635 by: Houghton, J. T., Ding, Y., Griggs, D. J., Noguer, M., van der Linden, L., Dai, X.,  
636 Maskell, K., and Johnson, C. A., Cambridge University Press, Cambridge, UK, 892,  
637 2001.

638 Etheridge, D. M., Steele, L. P., Langenfelds, R. L., Francey, R. J., Barnola, J. M., and  
639 Morgan, V. I.: Natural and anthropogenic changes in atmospheric CO<sub>2</sub> over the last 1000  
640 years from air in Antarctic ice and firn, *Journal of Geophysical Research: Atmospheres*,  
641 101, 4115-4128, 10.1029/95JD03410, 1996.

642 Fabry, V. J., Seibel, B. A., Feely, R. A., and Orr, J. C.: Impacts of ocean acidification on  
643 marine fauna and ecosystem processes, *ICES Journal of Marine Science: Journal du*  
644 *Conseil*, 65, 414-432, 10.1093/icesjms/fsn048, 2008.

645 Friedlingstein, P., Cox, P., Betts, R., Bopp, L., von Bloh, W., Brovkin, V., Cadule, P.,  
646 Doney, S., Eby, M., Fung, I., Bala, G., John, J., Jones, C., Joos, F., Kato, T., Kawamiya,  
647 M., Knorr, W., Lindsay, K., Matthews, H. D., Raddatz, T., Rayner, P., Reick, C.,  
648 Roeckner, E., Schnitzler, K. G., Schnur, R., Strassmann, K., Weaver, A. J., Yoshikawa,  
649 C., and Zeng, N.: Climate–Carbon Cycle Feedback Analysis: Results from the C4MIP  
650 Model Intercomparison, *Journal of Climate*, 19, 3337-3353, 10.1175/JCLI3800.1, 2006.  
651 Friedlingstein, P., Meinshausen, M., Arora, V. K., Jones, C. D., Anav, A., Liddicoat, S.  
652 K., and Knutti, R.: Uncertainties in CMIP5 Climate Projections due to Carbon Cycle  
653 Feedbacks, *Journal of Climate*, 27, 511-526, 10.1175/JCLI-D-12-00579.1, 2014.  
654 Fujieki, L., Santiago-Mandujano, F., Fumar, C., Liukas, R., and Church, M.: Hawaii  
655 Ocean Time-series Program Data Report, 2013.  
656 Fujino, J., Nair, R., Kainuma, M., Masui, T., and Matsuoka, Y.: Multi-gas mitigation  
657 analysis on stabilization scenarios using AIM global model, *Multigas Mitigation and*  
658 *Climate Policy*. The Energy Journal, Special Issue, 2006.  
659 Hansen, J., Sato, M., Ruedy, R., Nazarenko, L., Lacis, A., Schmidt, G. A., Russell, G.,  
660 Aleinov, I., Bauer, M., Bauer, S., Bell, N., Cairns, B., Canuto, V., Chandler, M., Cheng,  
661 Y., Del Genio, A., Faluvegi, G., Fleming, E., Friend, A., Hall, T., Jackman, C., Kelley,  
662 M., Kiang, N., Koch, D., Lean, J., Lerner, J., Lo, K., Menon, S., Miller, R., Minnis, P.,  
663 Novakov, T., Oinas, V., Perlwitz, J., Perlwitz, J., Rind, D., Romanou, A., Shindell, D.,  
664 Stone, P., Sun, S., Tausnev, N., Thresher, D., Wielicki, B., Wong, T., Yao, M., and  
665 Zhang, S.: Efficacy of climate forcings, *Journal of Geophysical Research: Atmospheres*,  
666 110, D18104, 10.1029/2005JD005776, 2005.  
667 Hartin, C. A., Bond-Lamberty, B., and Patel, P.: Projections of ocean acidification over  
668 three centuries using a carbonate chemistry box model, *Biogeosciences*, in prep.  
669 Harvey, L. D. D., and Schneider, S. H.: Transient climate response to external forcing on  
670 100–104 year time scales part 1: Experiments with globally averaged, coupled,  
671 atmosphere and ocean energy balance models, *Journal of Geophysical Research:*  
672 *Atmospheres*, 90, 2191-2205, 10.1029/JD090iD01p02191, 1985.  
673 Heron, M., Hanson, V., and Ricketts, I.: Open source and accessibility: advantages and  
674 limitations, *Journal of Interaction Science*, 1, 2, 10.1186/2194-0827-1-2, 2013.  
675 Hijioka, Y., Matsuoka, Y., Nishimoto, H., Masui, M., and Kainuma, M.: Global GHG  
676 emissions scenarios under GHG concentration stabilization targets, *Journal of*  
677 *Environmental Engineering*, 13, 97-108, 2008.  
678 Hoffert, M. I., Callegari, A. J., and Hsieh, C.-T.: The Role of Deep Sea Heat Storage in  
679 the Secular Response to Climatic Forcing, *J. Geophys. Res.*, 85, 6667-6679,  
680 10.1029/JC085iC11p06667, 1980.  
681 Holland, M. M., and Bitz, C. M.: Polar amplification of climate change in coupled  
682 models, *Climate Dynamics*, 21, 221-232, 10.1007/s00382-003-0332-6, 2003.  
683 Ince, D. C., Hatton, L., and Graham-Cumming, J.: The case for open computer programs,  
684 *Nature*, 482, 485-488, 2012.  
685 IPCC: *Climate Change 2001: The Science of Climate Change*. Contribution of Working  
686 Group I to the Second Assessment Report of the Intergovernmental Panel on Climate  
687 Change, Cambridge University Press, Cambridge, 2001.  
688 Irvine, P. J., Sriviver, R. L., and Keller, K.: Tension between reducing sea-level rise and  
689 global warming through solar-radiation management, *Nature Clim. Change*, 2, 97-100,



690 <http://www.nature.com/nclimate/journal/v2/n2/abs/nclimate1351.html#supplementary->  
691 [information](http://www.nature.com/nclimate/journal/v2/n2/abs/nclimate1351.html#supplementary-), 2012.

692 Joos, F., Prentice, I. C., Sitch, S., Meyer, R., Hooss, G., Plattner, G.-K., Gerber, S., and  
693 Hasselmann, K.: Global warming feedbacks on terrestrial carbon uptake under the  
694 Intergovernmental Panel on Climate Change (IPCC) Emission Scenarios, *Global*  
695 *Biogeochemical Cycles*, 15, 891-907, 10.1029/2000GB001375, 2001a.

696 Joos, F., Prentice, I. C., Sitch, S., Meyer, R., Hooss, G., Plattner, G.-K., Gerber, S., and  
697 Hasselmann, K.: Global warming feedbacks on terrestrial carbon uptake under the  
698 Intergovernmental Panel on Climate Change (IPCC) emission scenarios, *Global*  
699 *Biochemical Cycles*, 15, 891-907, 2001b.

700 Knox, F., and McElroy, M. B.: Changes in Atmospheric CO<sub>2</sub>: Influence of the Marine  
701 Biota at High Latitude, *J. Geophys. Res.*, 89, 4629-4637, 10.1029/JD089iD03p04629,  
702 1984.

703 Knutti, R., and Hegerl, G. C.: The equilibrium sensitivity of the Earth's temperature to  
704 radiation changes, *Nature Geosci*, 1, 735-743, 2008.

705 Le Quéré, C., Andres, R. J., Boden, T., Conway, T., Houghton, R. A., House, J. I.,  
706 Marland, G., Peters, G. P., van der Werf, G. R., Ahlström, A., Andrew, R. M., Bopp, L.,  
707 Canadell, J. G., Ciais, P., Doney, S. C., Enright, C., Friedlingstein, P., Huntingford, C.,  
708 Jain, A. K., Jourdain, C., Kato, E., Keeling, R. F., Klein Goldewijk, K., Levis, S., Levy,  
709 P., Lomas, M., Poulter, B., Raupach, M. R., Schwinger, J., Sitch, S., Stocker, B. D.,  
710 Viovy, N., Zaehle, S., and Zeng, N.: The global carbon budget 1959–2011, *Earth Syst.*  
711 *Sci. Data*, 5, 165-185, 10.5194/essd-5-165-2013, 2013.

712 Lenton, T. M.: Land and ocean carbon cycle feedback effects on global warming in a  
713 simple Earth system model, *Tellus B*, 52, 1159-1188, 10.1034/j.1600-0889.2000.01104.x,  
714 2000.

715 Lenton, T. M., Myerscough, R. J., Marsh, R., Livina, V. N., Price, A. R., and Cox, S. J.:  
716 Using GENIE to study a tipping point in the climate system, 1890, 871-884 pp., 2009.

717 Manne, A. S., and Richels, R. G.: Merge: an integrated assessment model for global  
718 climate change, *Energy and environment*, edited by: Loulou, R., Waub, J.-P., and  
719 Zaccour, G., Springer, New York, 2005.

720 Martin, R. C., Riehle, D., and Buschmann, F.: *Pattern Languages of Program Design 3*,  
721 Addison-Wesley, Boston, MA, 672 pp., 1997.

722 Meinshausen, M., Raper, S. C. B., and Wigley, T. M. L.: Emulating coupled atmosphere-  
723 ocean and carbon cycle models with a simpler model, *MAGICC6 – Part 1: Model*  
724 *description and calibration*, *Atmos. Chem. Phys.*, 11, 1417-1456, 10.5194/acp-11-1417-  
725 2011, 2011a.

726 Meinshausen, M., Smith, S. J., Calvin, K., Daniel, J. S., Kainuma, M. L. T., Lamarque, J.  
727 F., Matsumoto, K., Montzka, S. A., Raper, S. C. B., Riahi, K., Thomson, A., Velders, G.  
728 J. M., and Vuuren, D. P. P.: The RCP greenhouse gas concentrations and their extensions  
729 from 1765 to 2300, *Climatic Change*, 109, 213-241, 10.1007/s10584-011-0156-z, 2011b.

730 Meinshausen, M., Wigley, T. M. L., and Raper, S. C. B.: Emulating atmosphere-ocean  
731 and carbon cycle models with a simpler model, *MAGICC6 – Part 2: Applications*,  
732 *Atmos. Chem. Phys.*, 11, 1457-1471, 10.5194/acp-11-1457-2011, 2011c.

733 Morice, C. P., Kennedy, J. J., Rayner, N. A., and Jones, P. D.: Quantifying uncertainties  
734 in global and regional temperature change using an ensemble of observational estimates:

735 The HadCRUT4 data set, *Journal of Geophysical Research: Atmospheres*, 117, D08101,  
736 10.1029/2011JD017187, 2012.

737 Moss, R. H., Edmonds, J. A., Hibbard, K. A., Manning, M. R., Rose, S. K., van Vuuren,  
738 D. P., Carter, T. R., Emori, S., Kainuma, M., Kram, T., Meehl, G. A., Mitchell, J. F. B.,  
739 Nakicenovic, N., Riahi, K., Smith, S. J., Stouffer, R. J., Thomson, A. M., Weyant, J. P.,  
740 and Wilbanks, T. J.: The next generation of scenarios for climate change research and  
741 assessment, *Nature*, 463, 747-756,  
742 [http://www.nature.com/nature/journal/v463/n7282/suppinfo/nature08823\\_S1.html](http://www.nature.com/nature/journal/v463/n7282/suppinfo/nature08823_S1.html), 2010.

743 Murakami, K., Sasai, T., and Yamaguchi, Y.: A new one-dimensional simple energy  
744 balance and carbon cycle coupled model for global warming simulation, *Theoretical and  
745 Applied Climatology*, 101, 459-473, 10.1007/s00704-009-0232-8, 2010.

746 Myhre, G., Highwood, E. J., Shine, K. P., and Stordal, F.: New estimates of radiative  
747 forcing due to well mixed greenhouse gases, *Geophysical Research Letters*, 25, 2715-  
748 2718, 10.1029/98GL01908, 1998.

749 Nemani, R. R., Keeling, C. D., Hashimoto, H., Jolly, W. M., Piper, S. C., Tucker, C. J.,  
750 Myneni, R. B., and Running, S. W.: Climate-Driven Increases in Global Terrestrial Net  
751 Primary Production from 1982 to 1999, *Science*, 300, 1560-1563,  
752 10.1126/science.1082750, 2003.

753 Nordhaus, W. D.: A question of balance weighing the options on global warming  
754 policies, Yale University Press, New Haven, 2008.

755 Piao, S., Sitch, S., Ciais, P., Friedlingstein, P., Peylin, P., Wang, X., Ahlström, A., Anav,  
756 A., Canadell, J. G., Cong, N., Huntingford, C., Jung, M., Levis, S., Levy, P. E., Li, J.,  
757 Lin, X., Lomas, M. R., Lu, M., Luo, Y., Ma, Y., Myneni, R. B., Poulter, B., Sun, Z.,  
758 Wang, T., Viovy, N., Zaehle, S., and Zeng, N.: Evaluation of terrestrial carbon cycle  
759 models for their response to climate variability and to CO<sub>2</sub> trends, *Global Change  
760 Biology*, 19, 2117-2132, 10.1111/gcb.12187, 2013.

761 Pietsch, S. A., and Hasenauer, H.: Evaluating the self-initialization procedure for large-  
762 scale ecosystem models, *Global Change Biology*, 12, 1-12, 10.1111/j.1365-  
763 2486.2006.01211.x 2006.

764 Raper, S. C., Gregory, J. M., and Stouffer, R. J.: The Role of Climate Sensitivity and  
765 Ocean Heat Uptake on AOGCM Transient Temperature Response, *Journal of Climate*,  
766 15, 124-130, 2002.

767 Raper, S. C. B., Gregory, J. M., and Osborn, T. J.: Use of an upwelling-diffusion energy  
768 balance climate model to simulate and diagnose A/OGCM results, *Climate Dynamics*, 17,  
769 601-613, 2001.

770 Ratto, M., Castelletti, A., and Pagano, A.: Emulation techniques for the reduction and  
771 sensitivity analysis of complex environmental models, *Environmental Modelling and  
772 Software*, 34, 1-4, 2012.

773 Riahi, K., Grubler, A., and Nakicenovic, N.: Scenarios of long-term socio-economic and  
774 environmental development under climate stabilization, *Technological Forecasting and  
775 Social Change*, 74, 887-935, 2007.

776 Ricciuto, D. M., Davis, K. J., and Keller, K.: A Bayesian calibration of a simple carbon  
777 cycle model: The role of observations in estimating and reducing uncertainty, *Global  
778 Biogeochemical Cycles*, 22, GB2030, 10.1029/2006GB002908, 2008.

779 Rogner, H. H.: An assessment of world hydrocarbon resources, *Annual Review of  
780 Energy and the Environment*, 22, 217-262, 10.1146/annurev.energy.22.1.217, 1997.

781 Schlesinger, M. E., and Jiang, X.: Simple Model Representation of Atmosphere-Ocean  
782 GCMs and Estimation of the Time Scale of CO<sub>2</sub>-Induced Climate Change, *Journal of*  
783 *Climate*, 3, 1297-1315, 10.1175/1520-0442(1990)003<1297:SMROAO>2.0.CO;2, 1990.  
784 Senior, C. A., and Mitchell, J. F. B.: The time-dependence of climate sensitivity,  
785 *Geophysical Research Letters*, 27, 2685-2688, 10.1029/2000GL011373, 2000.  
786 Smith, S., and Wigley, T.: Multi-Gas Forcing Stabilization with the MiniCAM, *Energy*  
787 *Journal Special Issue #3*, 373-391, 2006.  
788 Smith, S. J., and Bond, T. C.: Two hundred fifty years of aerosols and climate: the end of  
789 the age of aerosols, *Atmos. Chem. Phys. Discuss.*, 13, 6419-6453, 10.5194/acp-14-537-  
790 2014, 2014.  
791 Sokolov, A. P., CA, S., S, D., S, P., DW, K., HD, J., RG, P., CE, F., JM, R., C, W., B, F.,  
792 MC, S., J, S., PH, S., M, J., and J, C.: The MIT Integrated Global System Model (IGSM)  
793 version 2: model description and baseline evaluation, MIT, Cambridge, 2005.  
794 Sriver, R., Urban, N., Olson, R., and Keller, K.: Toward a physically plausible upper  
795 bound of sea-level rise projections, *Climatic Change*, 115, 893-902, 10.1007/s10584-012-  
796 0610-6, 2012.  
797 Stocker, T.: Model Hierarchy and Simplified Climate Models, in: *Introduction to Climate*  
798 *Modelling, Advances in Geophysical and Environmental Mechanics and Mathematics*,  
799 Springer Berlin Heidelberg, 25-51, 2011.  
800 Takahashi, T., Sutherland, S. C., Wanninkhof, R., Sweeney, C., Feely, R. A., Chipman,  
801 D. W., Hales, B., Friederich, G., Chavez, F., Sabine, C., Watson, A., Bakker, D. C. E.,  
802 Schuster, U., Metzl, N., Yoshikawa-Inoue, H., Ishii, M., Midorikawa, T., Nojiri, Y.,  
803 Körtzinger, A., Steinhoff, T., Hoppema, M., Olafsson, J., Arnarson, T. S., Tilbrook, B.,  
804 Johannessen, T., Olsen, A., Bellerby, R., Wong, C. S., Delille, B., Bates, N. R., and de  
805 Baar, H. J. W.: Climatological mean and decadal change in surface ocean pCO<sub>2</sub>, and net  
806 sea-air CO<sub>2</sub> flux over the global oceans, *Deep Sea Research Part II: Topical Studies in*  
807 *Oceanography*, 56, 554-577, <http://dx.doi.org/10.1016/j.dsr2.2008.12.009>, 2009.  
808 Tanaka, K., Kriegler, E., Bruckner, T., Hooss, C., Knorr, W., and Raddatz, T.:  
809 Aggregated Carbon Cycle, Atmospheric Chemistry, and Climate Model (ACC2) -  
810 description of the forward and inverse models, Max Planck Institute for Meteorology.  
811 Hamburg, Germany, 188, 2007a.  
812 Tanaka, K., Kriegler, E., Bruckner, T., Hooss, G., Knorr, W., Raddatz, T. J., and Tol, R.:  
813 Aggregated carbon cycle, atmospheric chemistry, and climate model (ACC2), Hamburg,  
814 188, 2007b.  
815 Taylor, K. E., Stouffer, R. J., and Meehl, G. A.: An Overview of CMIP5 and the  
816 Experiment Design, *Bulletin of the American Meteorological Society*, 93, 485-498,  
817 10.1175/BAMS-D-11-00094.1, 2012.  
818 Urban, N. M., and Keller, K.: Complementary observational constraints on climate  
819 sensitivity, *Geophysical Research Letters*, 36, L04708, 10.1029/2008GL036457, 2009.  
820 Urban, N. M., and Keller, K.: Probabilistic hindcasts and projections of the coupled  
821 climate, carbon cycle and Atlantic meridional overturning circulation system: a Bayesian  
822 fusion of century-scale observations with a simple model, *Tellus A*, 62, 737-750,  
823 10.1111/j.1600-0870.2010.00471.x, 2010.  
824 van Vuuren, D., Elzen, M. J., Lucas, P., Eickhout, B., Strengers, B., Ruijven, B., Wonink,  
825 S., and Houdt, R.: Stabilizing greenhouse gas concentrations at low levels: an assessment

826 of reduction strategies and costs, *Climatic Change*, 81, 119-159, 10.1007/s10584-006-  
827 9172-9, 2007.

828 van Vuuren, D., Lowe, J., Stehfest, E., Gohar, L., Hof, A., Hope, C., Warren, R.,  
829 Meinshausen, M., and Plattner, G.-K.: How well do integrated assessment models  
830 simulate climate change?, *Climatic Change*, 104, 255-285, 10.1007/s10584-009-9764-2,  
831 2011.

832 Ward, D. S., and Mahowald, N. M.: Contributions of developed and developing countries  
833 to global climate forcing and surface temperature change, *Environmental Research*  
834 *Letters*, 9, 074008, 2014.

835 Wigley, T. M. L.: A simple inverse carbon cycle model, *Global Biogeochemical Cycles*,  
836 5, 373-382, 10.1029/91GB02279, 1991.

837 Wigley, T. M. L.: Global-mean temperature and sea level consequences of greenhouse  
838 gas concentration stabilization, *Geophysical Research Letters*, 22, 45-48,  
839 10.1029/94GL01011, 1995.

840 Wigley, T. M. L., Richels, R., and Edmonds, J. A.: Economic and environmental choices  
841 in the stabilization of atmospheric CO<sub>2</sub> concentrations, *Nature*, 379, 240-243, 1996.

842 Wigley, T. M. L., Smith, S. J., and Prather, M. J.: Radiative Forcing Due to Reactive Gas  
843 Emissions, *Journal of Climate*, 15, 2690-2696, 10.1175/1520-  
844 0442(2002)015<2690:RFDTRG>2.0.CO;2, 2002.

845 Wise, M., Calvin, K., Thomson, A., Clarke, L., Bond-Lamberty, B., Sands, R., Smith, S.  
846 J., Janetos, A., and Edmonds, J.: Implications of Limiting CO<sub>2</sub> Concentrations for Land  
847 Use and Energy, *Science*, 324, 1183-1186, 10.1126/science.1168475, 2009.

848 Wolkovich, E. M., Regetz, J., and O'Connor, M. I.: Advances in global change research  
849 require open science by individual researchers, *Global Change Biology*, 18, 2102-2110,  
850 10.1111/j.1365-2486.2012.02693.x, 2012.

851 Zeebe, R. E., and Wolf-Gladrow, D.: CO<sub>2</sub> in Seawater: Equilibrium, Kinetics, Isotopes,  
852 Elsevier, 2001.

853

854

855 **Table and Figure Captions:**

856 **Table 1:** Initial model conditions prior to the spinup phase. Carbon values change  
 857 slightly after spinning up to a steady state.  
 858

Variable	Description	Initial Value	Units	Notes
*C <sub>atm</sub>	Atmospheric Carbon	588.1	PgC	Murakami(2010)
*C <sub>D</sub>	Detritus Carbon	55.0	PgC	Denman et al., (2007) Land carbon (detritus, soil and vegetation) totaling ~2300PgC
*C <sub>S</sub>	Soil Carbon	1782.0	PgC	
*C <sub>V</sub>	Vegetation Carbon	550.0	PgC	
C <sub>DO</sub>	Deep Ocean	26000.0	PgC	Denman et al., (2007) Ocean carbon (deep, intermediate and surface) totaling ~3800PgC **
C <sub>HL</sub>	Surface Ocean High Latitude	140.0	PgC	
C <sub>IO</sub>	Intermediate Ocean	8400.0	PgC	
C <sub>LL</sub>	Surface Ocean Low Latitude	770.0	PgC	
F <sub>L</sub>	Atmosphere-Land Carbon Flux	0.0	PgC yr <sup>-1</sup>	
F <sub>O</sub>	Atmosphere-Ocean Carbon Flux	0.0	PgC yr <sup>-1</sup>	
NPP <sub>0</sub>	Net Primary Production	50.0	PgC yr <sup>-1</sup>	Approximate global value. Nemani et al., (2003)
T <sub>G</sub>	Global Temperature Anomaly	0.0	°C	
T <sub>HL</sub>	Temperature of high latitude surface ocean box	2.0	°C	Lenton, (2000)
T <sub>LL</sub>	Temperature of low latitude surface ocean box	22.0	°C	Lenton, (2000)

859 \* parameters appearing in the input file.

860 \*\* in order to obtain a steady state in Hector, carbon values in the intermediate box are

861 less than reported Denman et al.,(2007).

862 **Table 2:** Model parameters for the land and ocean carbon components.

Variable	Description	Value	Notes
$f_{ds}$	annual fraction of detritus carbon that is transferred to soil	0.60	The following fractions ( $f$ ) were selected to be generally consistent with previous simple earth system models (e.g., Meinshausen et al., 2011a; Ricciuto et al., 2008; Murakami et al., 2010).
$*f_{ld}$	annual fraction of land use change flux from detritus	0.01	
$f_{ls}$	annual fraction of land use change flux from soil	0.89	
$*f_{lv}$	annual fraction of land use change flux from vegetation	0.10	
$*f_{nd}$	annual fraction of NPP carbon that is transferred to detritus	0.60	
$f_{ns}$	annual fraction of NPP carbon that is transferred to soil	0.05	
$*f_{nv}$	annual fraction of NPP carbon that is transferred to vegetation	0.35	
$f_{rd}$	annual fraction of respiration carbon that is transferred to detritus	0.25	
$f_{rs}$	annual fraction of respiration carbon that is transferred to soil	0.02	
$f_{vd}$	annual fraction of vegetation carbon that is transferred to detritus	0.034	
$f_{vs}$	annual fraction of vegetation carbon that is transferred to soil	0.001	
$*\beta$	Beta	0.36	
$*Q_{10}$	Q10 respiration	2.45	
$*T_H$	High-latitude circulation	$4.9e7 \text{ m}^3 \text{ s}^{-1}$	Tuned to give ~100 PgC from surface to deep
$*T_T$	Thermohaline circulation	$7.2e7 \text{ m}^3 \text{ s}^{-1}$	Tuned to give ~100

			PgC from surface to deep
*E <sub>ID</sub>	Water mass exchange – intermediate to deep	1.25e7 m <sup>3</sup> s <sup>-1</sup>	Lenton, 2000; Knox and McElroy, 1984
*E <sub>LI</sub>	Water mass exchange – low latitude to intermediate	2.0e8 m <sup>3</sup> s <sup>-1</sup>	Lenton, 2000; Knox and McElroy, 1984

863

864

\* parameters appearing in the input file.

865 **Table 3:** CMIP5 ESM models used within this study. We use the same suite of models as  
 866 found in Friedlingstein et al. (2014). Note, not all variables are reported for each model  
 867 under all scenarios.  
 868

Model	Model Name	Institute
bcc-csm1-1	Beijing Climate Center, Climate System Model, version 1.1	Beijing Climate Center, China Meteorological Administration, China
CanESM2 *	Second Generation Canadian Earth System Model	Canadian Center for Climate Modeling and Analysis, BC, Canada
CESM1-BGC *	Community Earth System Model, version 1.0-Biogeochemistry	National Center for Atmospheric Research, United States
GFDL-ESM2G	Geophysical Fluid Dynamic Laboratory Earth System Model with GOLD ocean component	Geophysical Fluid Dynamics Laboratory, United States
HadGEM2-ES	Hadley Centre Global Environmental Model, version 2 (Earth System)	Met Office Hadley Centre, United Kingdom
inmcm4	Institute of Numerical Mathematics Coupled Model, version 4.0	Institute of Numerical Mathematics, Russia
IPSL-CM5A-LR	L'Institut Pierre-Simon Laplace Coupled Model, version 5A, coupled with NEMO, low resolution	Institut Pierre Simon Laplace, France
MIROC-ESM *	Model for Interdisciplinary Research on Climate, Earth System Model	Atmosphere and Ocean Research Institute; National Institute for Environmental Studies, Japan Agency for Marine-Earth Science and Technology, Japan
MPI-ESM-LR	Max Planck Institute Earth System Model, low resolution	Max Planck Institute for Meteorology, Germany
MRI-ESM1 *	Meteorological Research Institute Earth System Model, version 1	Meteorological Research Institute Earth, Japan
NorESM1-ME *	Norwegian Earth System Model, version 1, intermediate	Norwegian Climate Center, Norway



resolution

\* Models used in emissions forced scenarios (esmhist and esmrp85).

869 **Table 4:** Root mean square error (RMSE) for Hector versus observations, CMIP5, and  
 870 MAGICC for atmospheric [CO<sub>2</sub>], surface temperature anomaly, radiative forcing, fluxes  
 871 of carbon (ocean and land), and low latitude surface ocean pH and delta change ( $\Delta$ ) for  
 872 atmospheric [CO<sub>2</sub>], surface temperature anomaly and radiative forcing for Hector,  
 873 CMIP5, observations, and MAGICC6.

		Historical 1850 - 2005				
Variable		Hector	Observations	MAGICC	CMIP5	Units
[CO <sub>2</sub> ]*	RMSE	--	2.85	2.95	2.21	ppmv
	$\Delta$	85.78	94.47	95.0	103.30	
temperature	RMSE	--	0.15	0.13	0.15	deg C
	$\Delta$	0.98	0.91	0.76	1.01	
Forcing	RMSE	--	--	0.39	--	W m <sup>-2</sup>
	$\Delta$	2.16	--	1.75	--	
Ocean Flux	RMSE	--	--	--	0.25	PgC yr <sup>-1</sup>
Land Flux	RMSE	--	--	--	1.27	PgC yr <sup>-1</sup>
pH	RMSE	--	--	--	0.004	unitless

\*[CO<sub>2</sub>] observations are an average of Law Dome and Mauna Loa.

		RCP 8.5 1850 - 2300				
Variable		Hector	MAGICC	CMIP5	Units	
[CO <sub>2</sub> ] *	RMSE	--	10.41	7.54	ppmv	
	$\Delta$	1557.91	1695.0	--		
temperature	RMSE	--	0.12	0.52	deg C	
	$\Delta$	9.58	8.05	10.57		
Forcing	RMSE	--	0.26	--	W m <sup>-2</sup>	
	$\Delta$	12.80	12.24	--		
Ocean Flux	RMSE	--	--	1.39	PgC yr <sup>-1</sup>	
Land Flux	RMSE	--	--	3.86	PgC yr <sup>-1</sup>	
pH	RMSE	--	--	0.003	unitless	

\*CMIP5 [CO<sub>2</sub>] only to 2100.

874

## RCP 8.5 2005 - 2300

Variable		Hector	MAGICC	CMIP5	Units
[CO <sub>2</sub> ]*	RMSE	--	10.07	7.23	ppmv
	Δ	1472.13	1600.0	--	
temperature	RMSE	--	0.09	0.58	deg C
	Δ	8.59	7.30	9.57	
Forcing	RMSE	--	0.03	--	W m <sup>-2</sup>
	Δ	10.65	10.49	--	
Ocean Flux	RMSE	--	--	1.41	PgC yr <sup>-1</sup>
Land Flux	RMSE	--	--	4.59	PgC yr <sup>-1</sup>
pH	RMSE	--	--	0.001	unitless

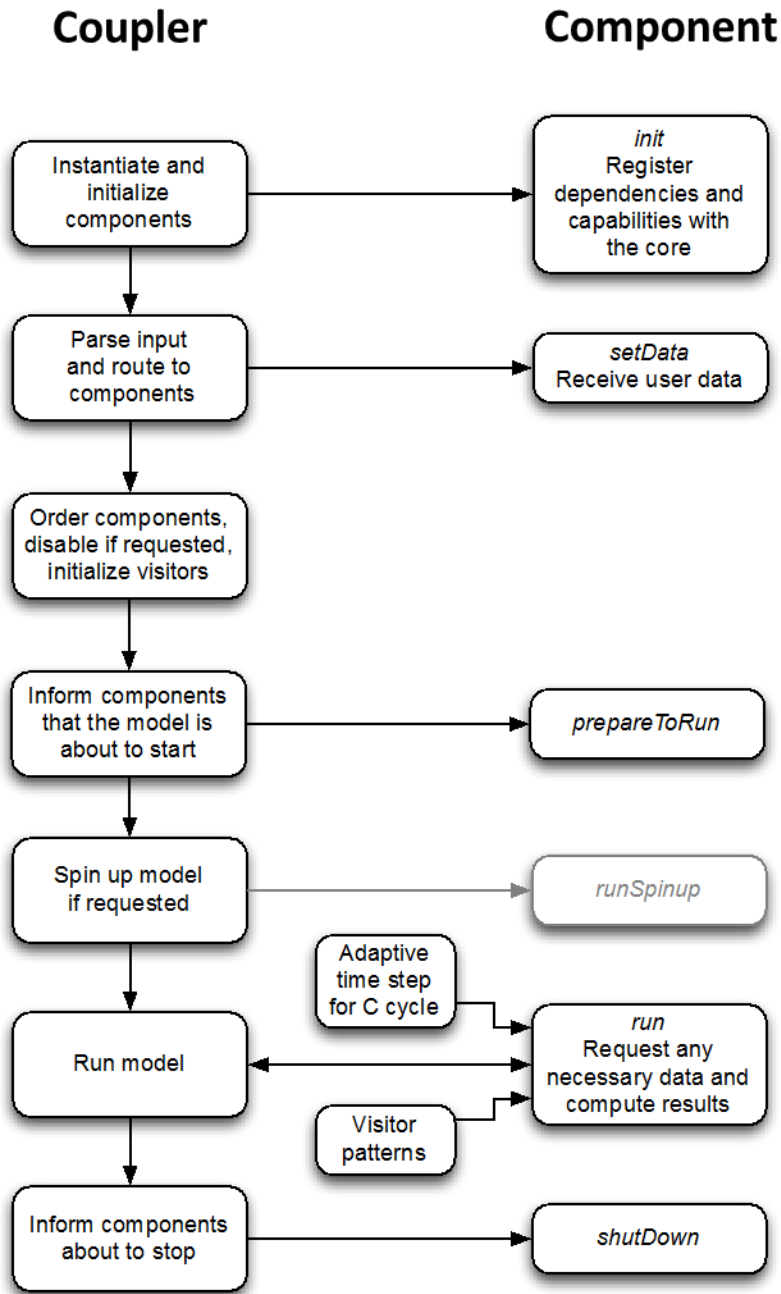
\*CMIP5 [CO<sub>2</sub>] only to 2100.

875

876

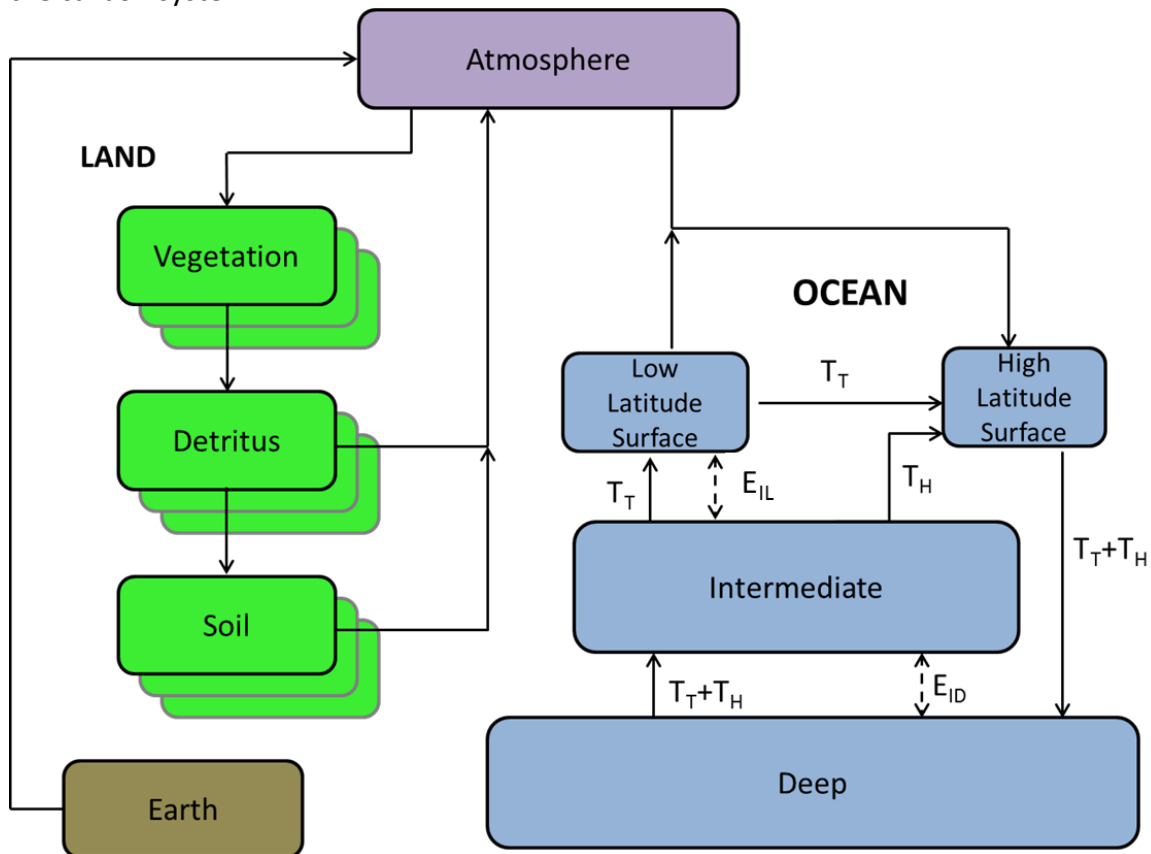
877

878 **Figure 1:** Model phases for the coupler (left) and a typical component (right). Arrows  
 879 show flow of control and data. The greyed spinup step is optional.



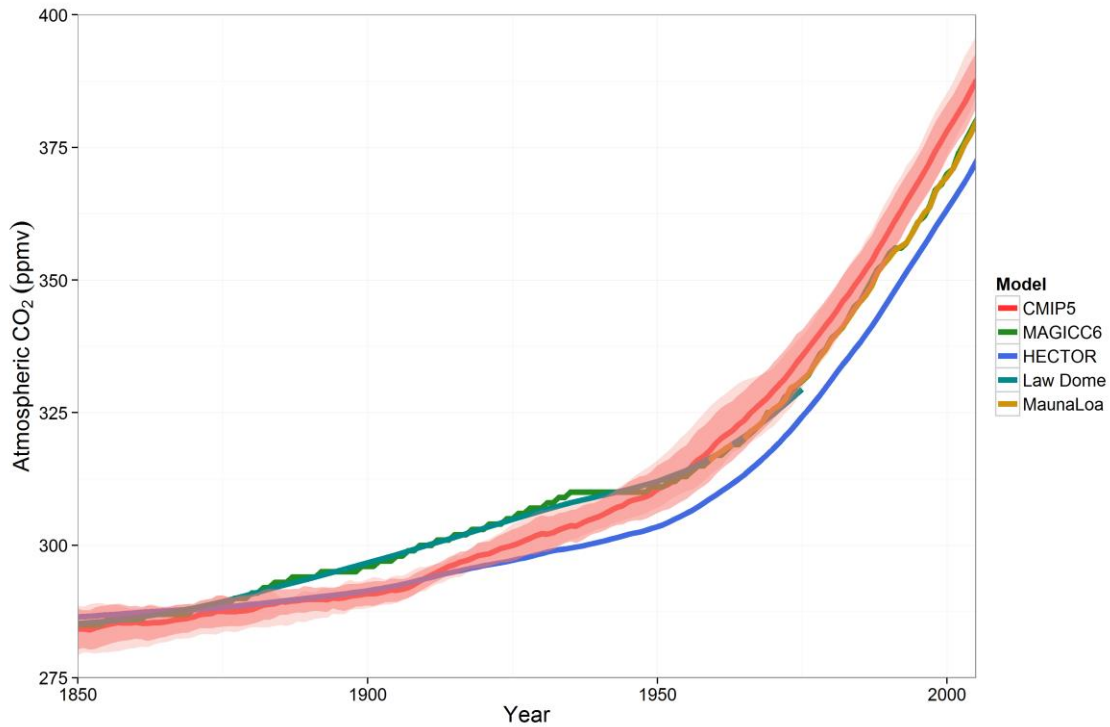
880  
881

882 **Figure 2:** Representation of Hector’s carbon cycle, land, atmosphere, and ocean. The  
 883 atmosphere consists of one well mixed box. The ocean consists of four boxes, with  
 884 advection and water mass exchange simulating thermohaline circulation (see Table 2 for  
 885 description of parameters). At steady state, the high latitude surface ocean takes up  
 886 carbon from the atmosphere, while the low latitude surface ocean off gases carbon to  
 887 the atmosphere. The land consists of a user defined number of biomes or regions for  
 888 vegetation, detritus and soil. At steady state the vegetation takes up carbon from the  
 889 atmosphere while the detritus and soil release carbon back into the atmosphere. The  
 890 earth pool is continually debited with each time step to act as a mass balance check on  
 891 the carbon system.



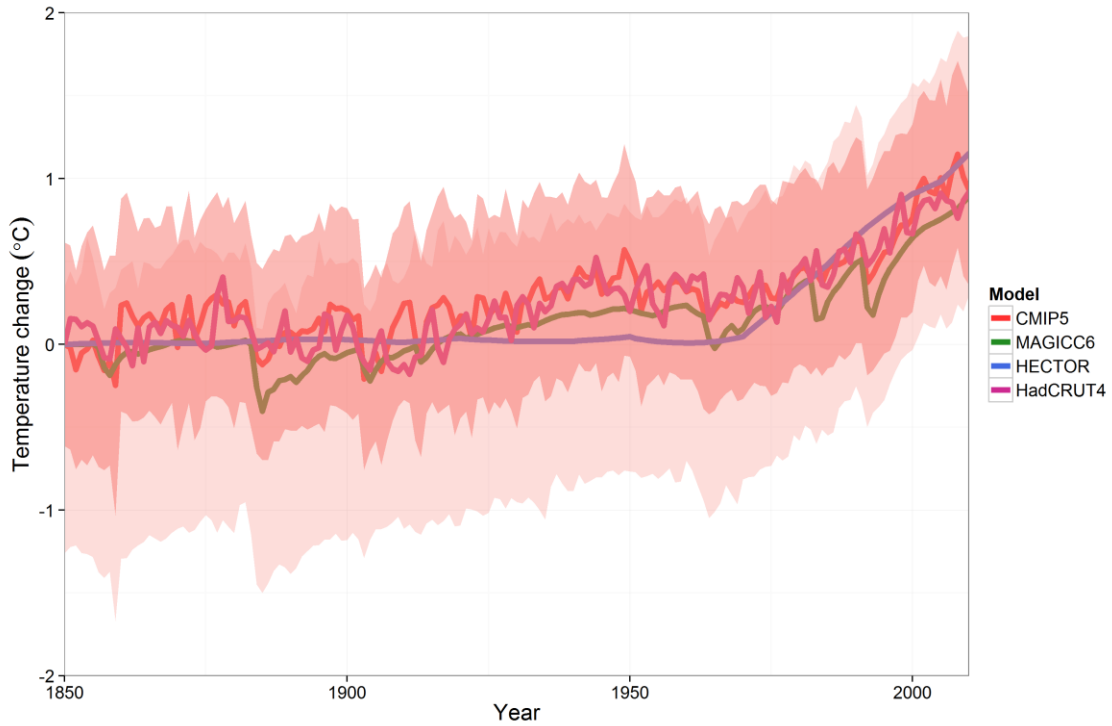
892  
 893  
 894

895 **Figure 3:** Historical atmospheric [CO<sub>2</sub>] from 1850 to 2005 for Hector (blue), CMIP5  
896 median, standard deviation, and model range (pink, n=4), MAGICC6 (green), Law Dome  
897 (teal), and Mauna Loa (brown). Note CMIP5 data are from the prescribed emissions  
898 historical scenario (esmHistorical). MAGICC6, however, is constrained to match the  
899 observational record. Although Hector can be run with similar constraints, in this study  
900 Hector was unconstrained to highlight the full performance of the model. n=4 is the  
901 number of CMIP5 models used to produce this figure.



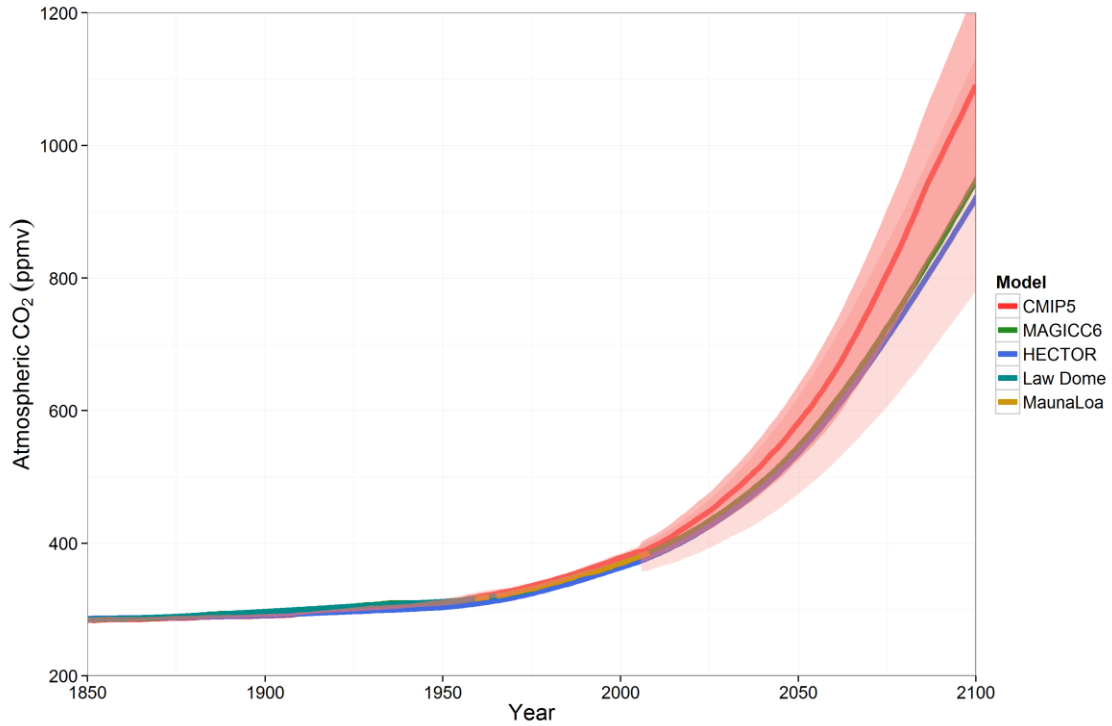
902  
903  
904

905 **Figure 4:** Historical global temperature anomaly relative to 1850 for Hector (blue),  
906 MAGICC6 (green), CMIP5 median, standard deviation and model range (pink, n=8), and  
907 historical observations from HadCRUT4 (purple). Hector is running without the effects of  
908 volcanic forcing, leading to a smoother representation of temperature with time.  
909



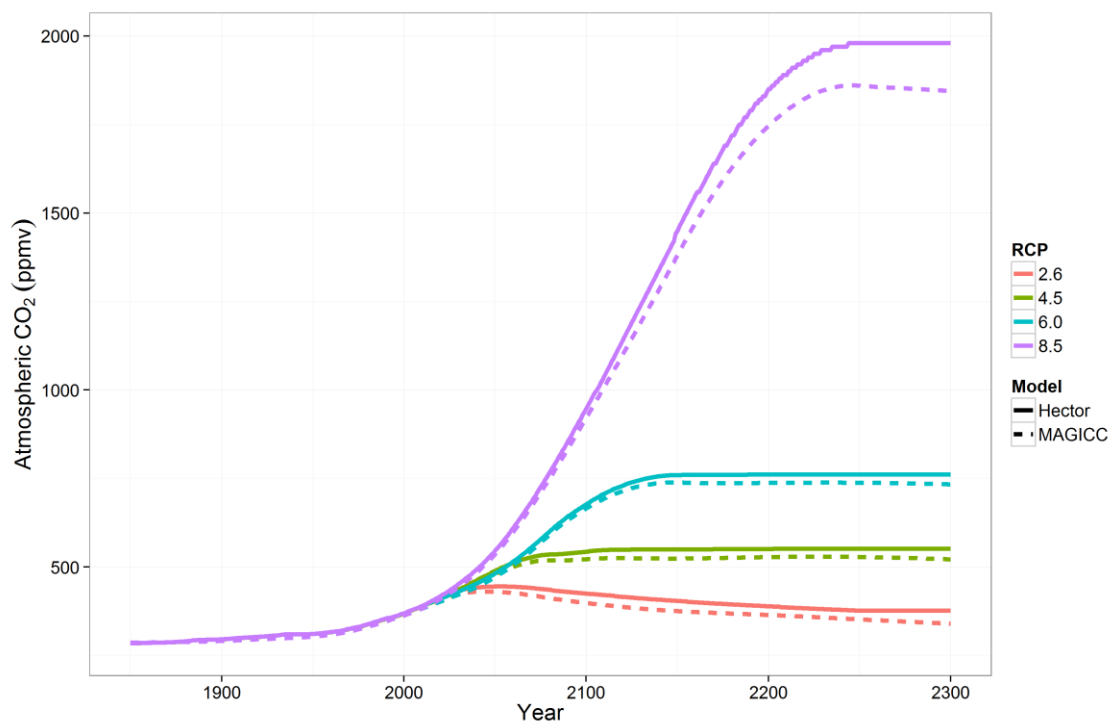
910

911 **Figure 5:** Atmospheric [CO<sub>2</sub>] from 1850 to 2100 under RCP 8.5 for Hector (blue),  
912 MAGICC6 (green), Mauna Loa (brown), Law Dome (teal) and esmRCP 8.5 (prescribed  
913 emissions scenario) CMIP5 median, one standard deviation and model range (pink, n=4  
914 (1850-2000) and n=5 (2001-2100)). Note that the CMIP5 models run under esmrcp85  
915 do not extend to 2300.



916  
917

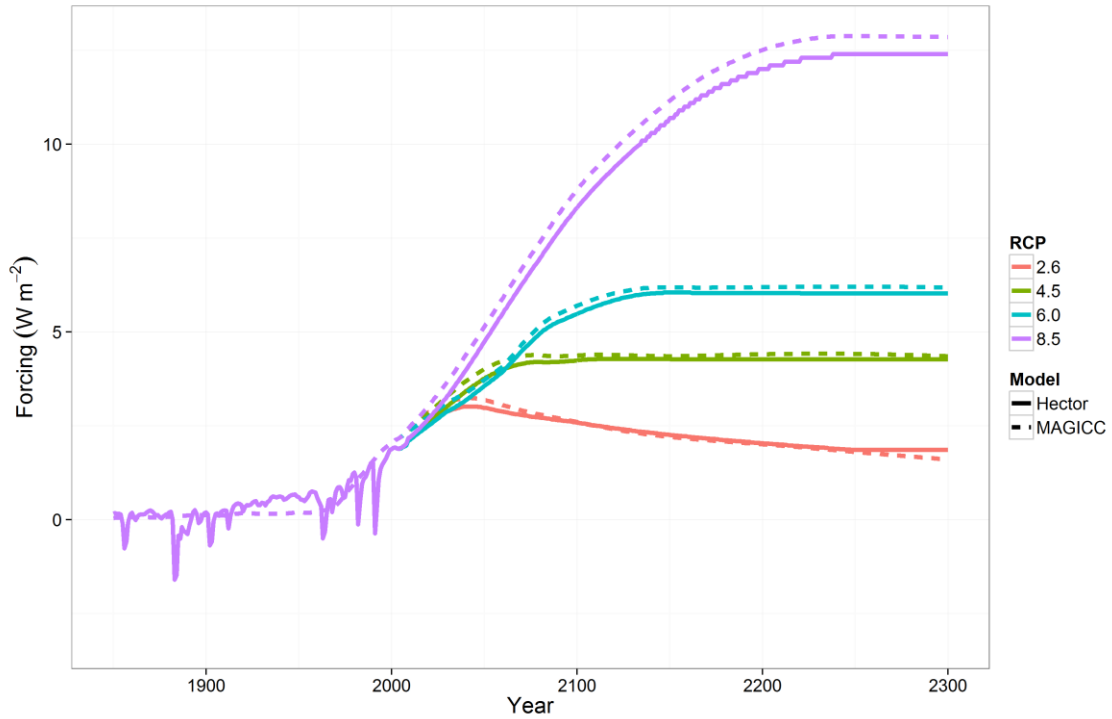
918 **Figure 6:** Atmospheric [CO<sub>2</sub>] from 1850 to 2300 for RCP 2.6 (red), RCP 4.5 (green), RCP  
919 6.0 (blue), RCP 8.5 (purple), Hector (solid) and MAGICC6 (dashed).  
920



921  
922

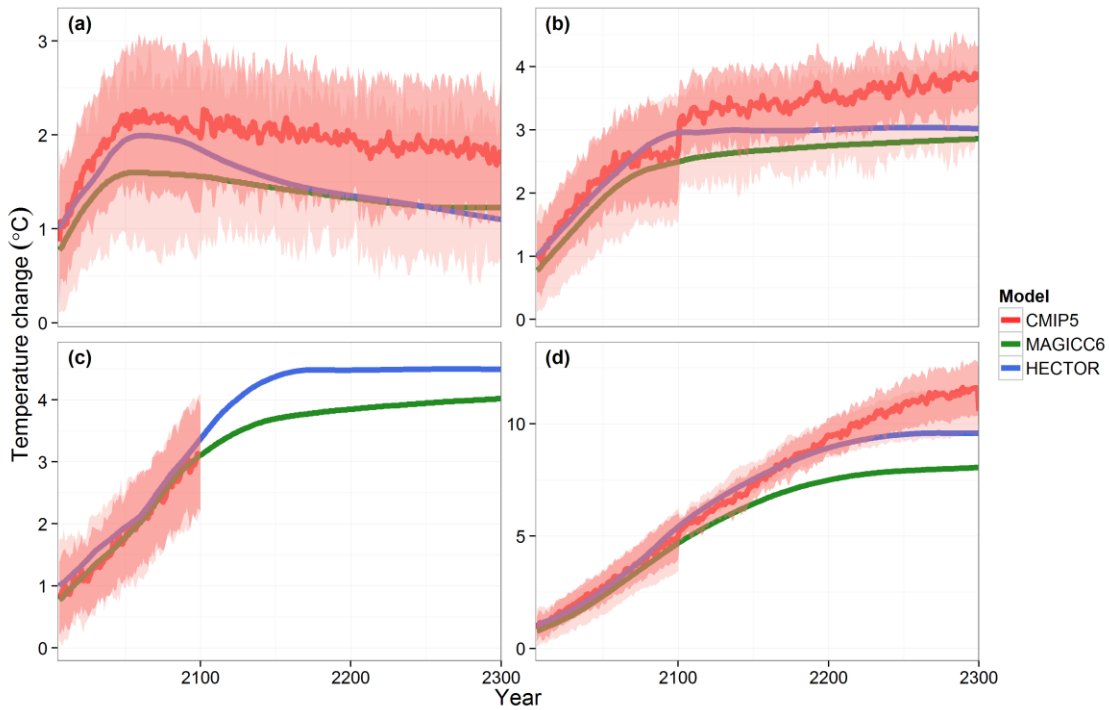


923 **Figure 7:** Relative radiative forcing from 1850 to 2300 for Hector (solid) and MAGICC6  
924 (dashed) for all four RCP scenarios, 2.6 (red), 4.5 (green), 6.0 (blue), 8.5 (purple). Hector  
925 has the option to enable or disable radiative forcing from historical volcanic emissions.  
926 We have opted to disable this for ease of comparison across all RCPs.  
927



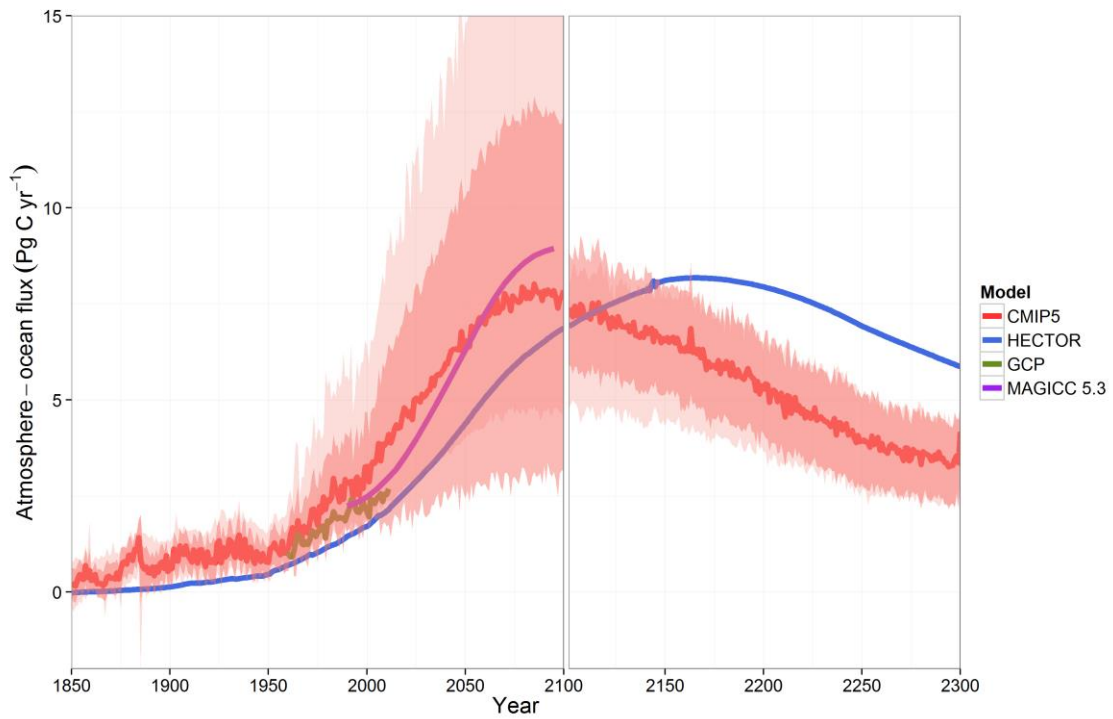
928  
929

930 **Figure 8:** Global temperature anomaly relative to 1850 for (a) RCP 2.6 (b) RCP 4.5 (c) RCP  
 931 6.0 and (d) RCP 8.5, comparing Hector (blue), MAGICC6 (green), and CMIP5 median,  
 932 standard deviation and model range (pink). The CMIP5 models under RCP 6.0 used in  
 933 this study do not extend to 2300. Note the change in scales between the four panels.  
 934 Number of CMIP5 models in a) n=7 (2006-2100) and n=5 (2101-2300), b) n=9 (2006-  
 935 2100) and n=6(2101-2300), c) n=6 (2006-2100), d) n=9 (2006-2100) and n=3 (2101-  
 936 2300).



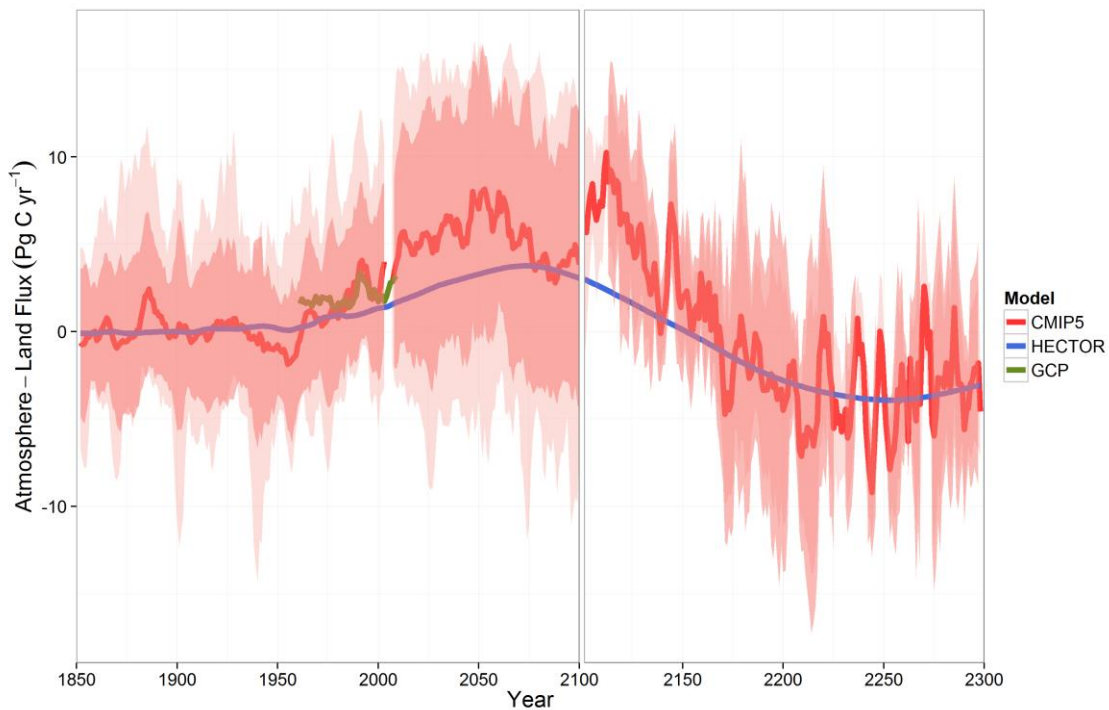
937  
 938

939 **Figure 9:** Global air-sea fluxes of carbon under RCP 8.5, Hector (blue), MAGICC5.3  
940 (purple, note that this is not the current version of MAGICC), CMIP5 median, standard  
941 deviation, and model range (pink, n=9 (1850-2100) and n=4 (2101-2300)), and  
942 observations from GCP (green) (Le Quéré et al., 2013). The break in the graph at 2100  
943 signifies a change in the number of models that ran the RCP 8.5 extension.



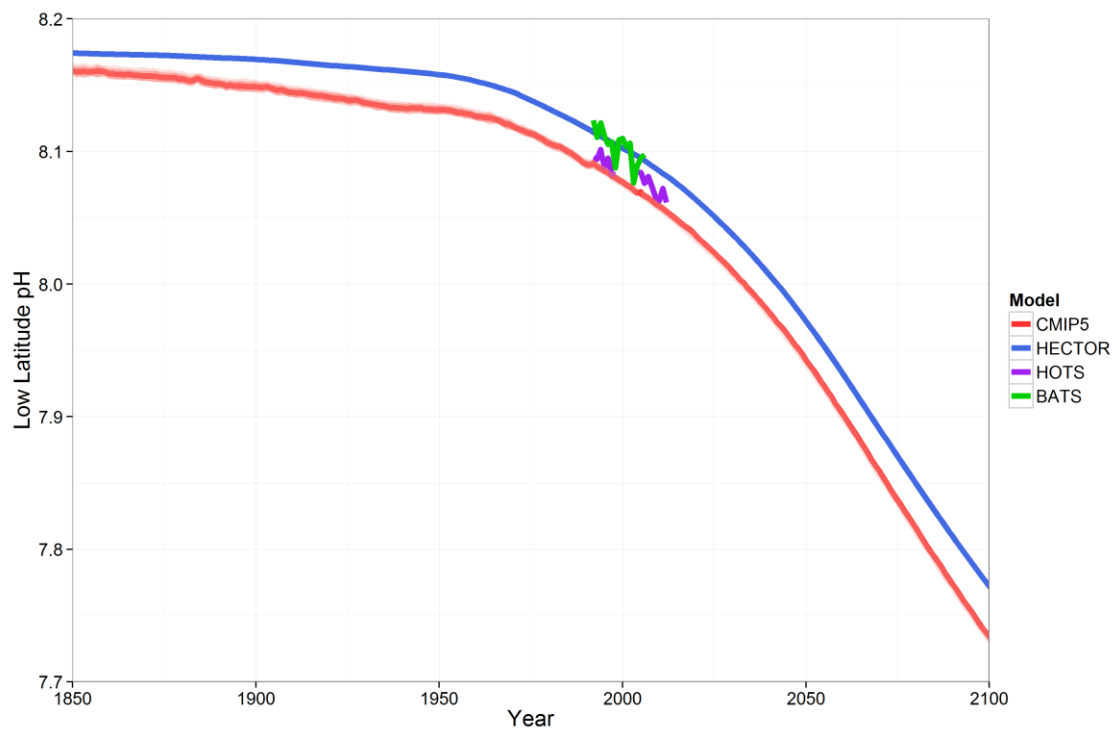
944  
945

946 **Figure 10:** Global air-land fluxes of carbon under RCP 8.5, Hector (blue), CMIP5 median,  
947 standard deviation, and model range (pink, n=8 (1850-2100) and n=2 (2101-2300)), and  
948 observations from GCP (green) (Le Quéré et al., 2013). The break in the graph at 2100  
949 signifies a change in the number of models that ran the RCP 8.5 extension.  
950



951

952 **Figure 11:** Low latitude (< 55) ocean pH for RCP 8.5, from 1850 – 2100, Hector (blue),  
953 CMIP5 median, standard deviation, and model range (pink, n=6) and observations from  
954 BATS (green) and HOTS (purple).  
955



956